Poly(ADP-ribosyl)ation links the chromatin remodeler SMARCA5/SNF2H to RNF168-dependent DNA damage signaling

Godelieve Smeenk[1,*], Wouter W. Wiegant[1,*], Jurgen A. Marteijn[2], Martijn S. Luijsterburg[1], Nicholas Sroczynski[3], Thomas Costelloe[1], Ron J. Romeijn[1], Albert Pastink[1], Niels Mailand[3], Wim Vermeulen[2] and Haico van Attikum[1,‡]

[1]Department of Toxicogenetics, Leiden University Medical Center, Einthovenweg 20, 2333 ZC, Leiden, The Netherlands
[2]Department of Genetics, Center for Biomedical Genetics, Erasmus Medical Center, 3015 GE, Rotterdam, The Netherlands
[3]Novo Nordisk Foundation Center for Protein Research, Faculty of Health Sciences, University of Copenhagen, 2200 Copenhagen, Denmark

*These authors contributed equally to this work
‡Author for correspondence (h.van.attikum@lumc.nl)

Accepted 3 December 2012
Journal of Cell Science 126, 889–903

doi: 10.1242/jcs.109413

Summary

Ionizing radiation (IR)-induced DNA double-strand breaks (DSBs) arising in native chromatin elicit an RNF8/RNF168-dependent ubiquitylation response, which triggers the recruitment of various repair factors. Precisely how this response is regulated in the context of chromatin remains largely unexplored. Here, we show that SMARCA5/SNF2H, the catalytic subunit of ISWI chromatin remodeling complexes, is recruited to DSBs in a poly(ADP-ribose) polymerase 1 (PARP1)-dependent manner. Remarkably, PARP activity, although dispensable for the efficient spreading of γH2AX into damaged chromatin, selectively promotes spreading of SMARCA5, the E3 ubiquitin ligase RNF168, ubiquitin conjugates and the ubiquitin-binding factors RAD18 and the RAP80–BRCA1 complex throughout DSB-flanking chromatin. This suggests that PARP regulates the spatial organization of the RNF168-driven ubiquitin response to DNA damage. In support of this, we show that SMARCA5 and RNF168 interact in a DNA damage- and PARP-dependent manner. RNF168 became poly(ADP-ribosyl)ated after DNA damage, while RNF168 and poly(ADP-ribose) chains were required for SMARCA5 binding *in vivo*, explaining how SMARCA5 is linked to the RNF168 ubiquitin cascade. Moreover, SMARCA5 was found to regulate the ubiquitin response by promoting RNF168 accumulation at DSBs, which subsequently facilitates efficient ubiquitin conjugation and BRCA1 assembly. Underlining the importance of these findings, we show that SMARCA5 depletion renders cells sensitive to IR and results in DSB repair defects. Our study unveils a functional link between DNA damage-induced poly(ADP-ribosyl)ation, SMARCA5-mediated chromatin remodeling and RNF168-dependent signaling and repair of DSBs.

Key words: SMARCA5/SNF2H, Chromatin remodeling, Poly(ADP-ribose) polymerase, PARP, RNF168, DNA damage signaling and repair

Introduction

Chromosomal DNA double-strand breaks (DSBs), which can be generated by exposure of cells to ionizing radiation (IR) or arise during DNA replication, are a major threat to genome stability. Inefficient or inaccurate repair of DSBs can lead to chromosome rearrangements, which may result in cancer development or cell death (Jackson and Bartek, 2009; Negrini et al., 2010). To circumvent the deleterious effects of DSBs, cells activate the DNA damage response (DDR), which comprises events that lead to detection and repair of these lesions, as well as delay in cell cycle progression (Huen and Chen, 2010). DSB repair involves two dedicated pathways known as non-homologous end-joining (NHEJ) and homologous recombination (HR) (Jackson and Bartek, 2009; Negrini et al., 2010; Wyman and Kanaar, 2006).

Numerous DDR proteins accumulate at IR-induced DSBs, forming cytologically discernible structures known as ionizing radiation-induced foci (IRIF) (Bekker-Jensen and Mailand, 2010; Huen and Chen, 2010). A key step in IRIF formation is the ATM/DNA-PK-mediated phosphorylation of histone H2AX (termed γH2AX). MDC1 subsequently binds γH2AX and mediates recruitment of the E3 ubiquitin ligases RNF8 and RNF168 together with HERC2 and the E2 ubiquitin conjugase UBC13. The ensuing chromatin ubiquitylation catalyzed by RNF8/RNF168/HERC2/UBC13 promotes recruitment of several proteins, including BRCA1 and 53BP1, culminating in checkpoint activation and DNA repair (Bekker-Jensen et al., 2010; Doil et al., 2009; Huen et al., 2007; Mailand et al., 2007; Stewart et al., 2009; Wang et al., 2007). Recent studies also implicated several ubiquitin ligases, such as TRIP12 and UBR5, as antagonists of the RNF168-driven ubiquitin response, preventing excessive spreading of DSB response factors to undamaged chromosomes (Gudjonsson et al., 2012).

Efficient signaling and repair of DSBs is hampered by the packaging of genomic DNA, through histone and non-histone proteins, into chromatin. Histones are extensively modified in response to DNA damage and it is becoming clear that the crosstalk between histone modifications in DSB-flanking chromatin controls the DDR (Luijsterburg et al., 2012a; van Attikum and Gasser, 2009). However, how this is accomplished remains largely elusive. Recent studies have begun to explore this

in mammalian cells and demonstrated that the TIP60 and SWI/SNF chromatin remodeling complexes facilitate DSB repair by promoting histone acetylation and H2AX phosphorylation at DSBs, respectively (Lee et al., 2010; Murr et al., 2006; Park et al., 2006). p400 and CHD4, the catalytic subunits of the TIP60 and NuRD chromatin remodeling complexes, respectively, not only facilitate DSB repair, but also promote the RNF8/RNF168 ubiquitin response at DSBs (Larsen et al., 2010; Luijsterburg et al., 2012a; Smeenk et al., 2010; Xu et al., 2010). It was shown that p400 recruitment to DSBs is regulated by MDC1 (Xu et al., 2010), while CHD4 is recruited by RNF8, suggesting that distinct DSB response factors recruit specific chromatin remodeling activities at the various stages of the DSB response, possibly to optimally reconfigure the chromatin structure for each step of this process (Luijsterburg and van Attikum, 2011). However, whether more downstream factors, such as RNF168 or BRCA1, also require chromatin-modifying activities is not known. Recently it was found that SMARCA5/SNF2H, the ATPase of several distinct ISWI chromatin remodeling complexes, is also involved in the DSB response (Lan et al., 2010; Nakamura et al., 2011; Sánchez -Molina et al., 2011). However, mechanistic insight into how SMARCA5 affects the signaling and repair of DSBs is currently limited. Here we uncover a novel functional link between poly(ADP-ribosyl)ation, SMARCA5-mediated chromatin remodeling and the RNF168-dependent signaling process in the DDR.

Results

SMARCA5 protects human cells against IR

A genome-wide RNAi screen in *Caenorhabditis elegans* identified 45 genes, including known DDR factors, as well as novel genes such as *isw-1*, which protect worms against IR (van Haaften et al., 2006). Database searches revealed two human proteins, SMARCA1/SNF2L (63% identity and 79% similarity) and SMARCA5/SNF2H (64% identity and 79% similarity), highly homologous to *C. elegans* ISW-1. Both proteins are members of the ISWI subclass of the SNF2 ATPase family (Bao and Shen, 2007), and are catalytic subunits of ATP-dependent chromatin remodeling complexes (Barak et al., 2003; Collins et al., 2002; Ito et al., 1999; LeRoy et al., 2000; Poot et al., 2000). In this study we examined the role of SMARCA5 in the DSB response. Based on the findings in *C. elegans*, we first tested whether SMARCA5 knockdown affects clonogenic survival of mammalian cells after exposure to IR. In agreement with a previous study (Lan et al., 2010), we found that RNAi-mediated SMARCA5 depletion markedly increased IR sensitivity to the same extent as depletion of XRCC4 or ATM (Fig. 1A,B; supplementary material Fig. S1A,B).

SMARCA5 is required for DSB repair by NHEJ

To assess the involvement of SMARCA5 in IR-induced DSB rejoining, we used the neutral comet assay. DSB levels were slightly elevated in non-irradiated SMARCA5-depleted cells, suggesting that SMARCA5 may prevent spontaneous chromosome breakage (supplementary material Fig. S1C,D, −IR samples). Importantly, IR treatment induced similar DSB levels in SMARCA5-depleted cells and control cells (supplementary material Fig. S1C,D, 0 h timepoint). Conversely, DSB levels were significantly higher 2 h after IR in SMARCA5-knockdown cells compared to control cells, but nearly returned to levels observed in control cells at 6 h (supplementary material Fig. S1C,D). Thus, SMARCA5 loss attenuates the rate of DSB repair, which in turn may affect cell cycle progression. Indeed, SMARCA5-depleted cells accumulated in the G2 phase after IR, but, in contrast to control cells, failed to recover from this arrest (supplementary material Fig. S1E,F). These results suggest that SMARCA5 promotes DSB repair.

To assess a possible role of SMARCA5 in NHEJ, we employed the EJ5-GFP reporter system, which measures repair between two tandem I-S*ce*I sites that separate a *GFP* gene from its promoter. Following I-S*ce*I expression, repair of the two I-S*ce*I-induced DSBs by NHEJ fuses the promoter to the *GFP* coding sequence and restores GFP expression (supplementary material Fig. S2A) (Bennardo et al., 2008). As expected, loss of the NHEJ factor XRCC4, but not of the HR factor BRCA2, reduced the efficiency of NHEJ as measured by GFP fluorescence (Fig. 1C). Interestingly, SMARCA5 depletion impaired NHEJ to the same extent as XRCC4 knockdown (Fig. 1C). Cell cycle profiles were not altered in these cells, ruling out any effect of cell cycle changes on the NHEJ efficiency (supplementary material Fig. S2D). Hence, our results strongly suggest that SMARCA5 promotes DSB repair by NHEJ.

SMARCA5 is required for DSB repair by HR

Next we assessed a possible role of SMARCA5 in HR by using the DR-GFP reporter system. In this system, a single I-S*ce*1 site is present in one of two defective GFP reporter genes. Following I-S*ce*1 expression, repair of the I-S*ce*I-induced DSB by gene conversion produces a functional *GFP* gene (supplementary material Fig. S2B) (Weinstock et al., 2006). As expected, BRCA2 depletion dramatically reduced HR efficiency (Fig. 1D; supplementary material Fig. S2B,C) (Moynahan et al., 2001). Remarkably, SMARCA5 depletion induced a similar reduction in HR repair (Fig. 1D; supplementary material Fig. S2C). As cell cycle profiles remained unchanged in these cells, we can rule out that cell cycle changes affected the HR efficiency (supplementary material Fig. S2D). HR-deficient cells confer extreme sensitivity to Poly(ADP-ribose) polymerase (PARP) inhibitors (McCabe et al., 2006). Consistent with a role in HR, clonogenic survival assays revealed an enhanced sensitivity of SMARCA5-depleted cells to PARP inhibitor (PARPi), comparable to that observed after BRCA2 depletion (Fig. 1E). Thus, in line with previous studies (Lan et al., 2010; Nakamura et al., 2011), our results suggest that SMARCA5 is required for DSB repair by NHEJ and HR.

SMARCA5 is rapidly recruited to DSBs

Recent work reported that SMARCA5 is recruited to DNA damage sites (Erdel et al., 2010; Lan et al., 2010; Nakamura et al., 2011; Sánchez-Molina et al., 2011). Chromatin immunoprecipitation (ChIP) coupled to quantitative PCR (qPCR) confirmed these results by showing SMARCA5 and γH2AX accumulation at two different sites flanking A*si*SI-induced DSBs on chromosome 1 and 22 (supplementary material Fig. S3A–D) (Iacovoni et al., 2010). Moreover, we also found that SMARCA5-GFP accumulates in multiphoton laser-induced tracks and spanned the entire chromatin region marked by γH2AX or RAD51 (Fig. 1F). Notably, the nucleotide excision repair protein XPA, did not accumulate, suggesting that the applied laser settings primarily create DNA strand breaks (Fig. 2A). SMARCA5-GFP rapidly accumulated, reaching maximum levels around 3–5 minutes ($t_{1/2}$=40 s), and bound SMARCA5 could be detected in the DSB-containing chromatin compartment for at least 2 hours (Fig. 2A,B;

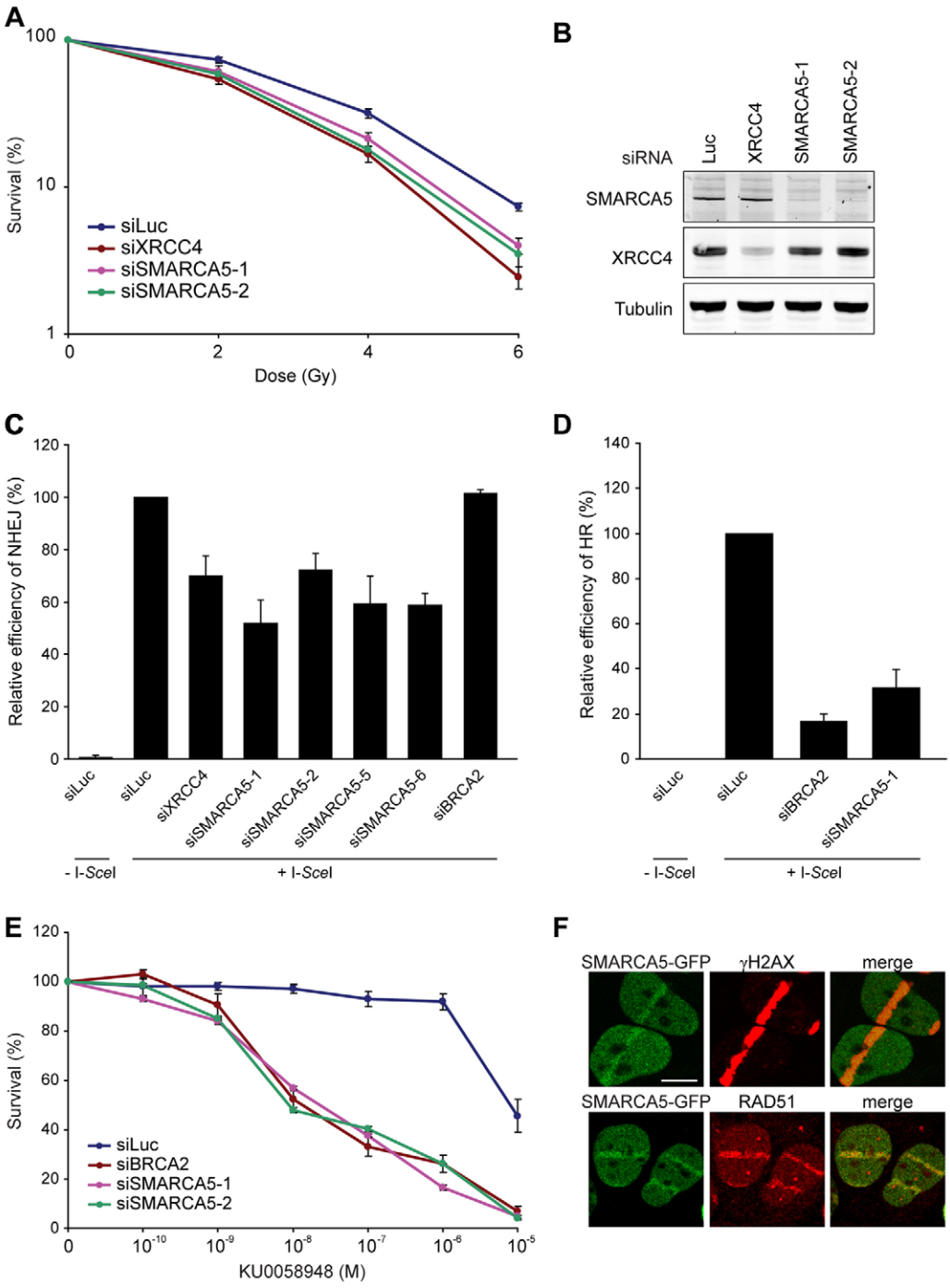

Fig. 1. SMARCA5 protects cells against IR and is recruited to DSBs to promote DNA repair. (**A**) VH10-SV40 cells were transfected with the indicated siRNAs, exposed to IR and scored for clonogenic survival. Values are means ± s.e.m. of three independent experiments. (**B**) SMARCA5 and XRCC4 levels were monitored by western blot analysis using whole cell extracts (WCE) of cells in A. Tubulin was used as a loading control. (**C**) HEK293T cells containing the NHEJ reporter EJ5–GFP were transfected with the indicated siRNAs and 48 h later transfected with an I-*Sce*I expression vector (pCBASce). Knockdown efficiency for the indicated siRNAs is shown in B and supplementary material Fig. 8B. Values are means ± s.e.m. of three experiments is shown. (**D**) As in C, except that cells containing the HR reporter DR–GFP were used. Knockdown efficiency for the indicated siRNAs is shown in B and supplementary material Fig. S2C. (**E**) As in A, except that cells were treated with PARPi. (**F**) U2OS cells expressing SMARCA5–GFP were subjected to multiphoton laser irradiation. After 15 min cells were immunostained for γH2AX and RAD51. Scale bar: 10 µm.

supplementary material Fig. S3E). Finally, kinetic studies show that SMARCA5-GFP accumulates at laser-inflicted DNA damage with similar kinetics to GFP-MDC1, while the recruitment of 53BP1 is considerably slower (Fig. 2A,B).

PARP contributes to SMARCA5 recruitment to DSBs

Previous work implicated a role for the RNF20 E3 ubiquitin ligase in the recruitment of SMARCA5 to DSBs (Nakamura et al., 2011). It remains, however, unclear whether other factors regulate SMARCA5 assembly at DNA strand breaks. Since ATM and DNA-PK play key roles in the DSB response (Jackson and Bartek, 2009; Luijsterburg and van Attikum, 2011; van Attikum and Gasser, 2009), we examined whether their chemical inhibition impacts SMARCA5 assembly at DSBs-tracks. Although ATM and DNA/PK inhibition prevented robust γH2AX IRIF formation and reduced γH2AX accumulation in laser-tracks, it did not affect SMARCA5 accumulation (Fig. 2C,D; supplementary material Fig. S4A–D).

Recently it was shown that PARP1, which binds to DNA strand breaks and catalyzes the attachment of PAR chains on

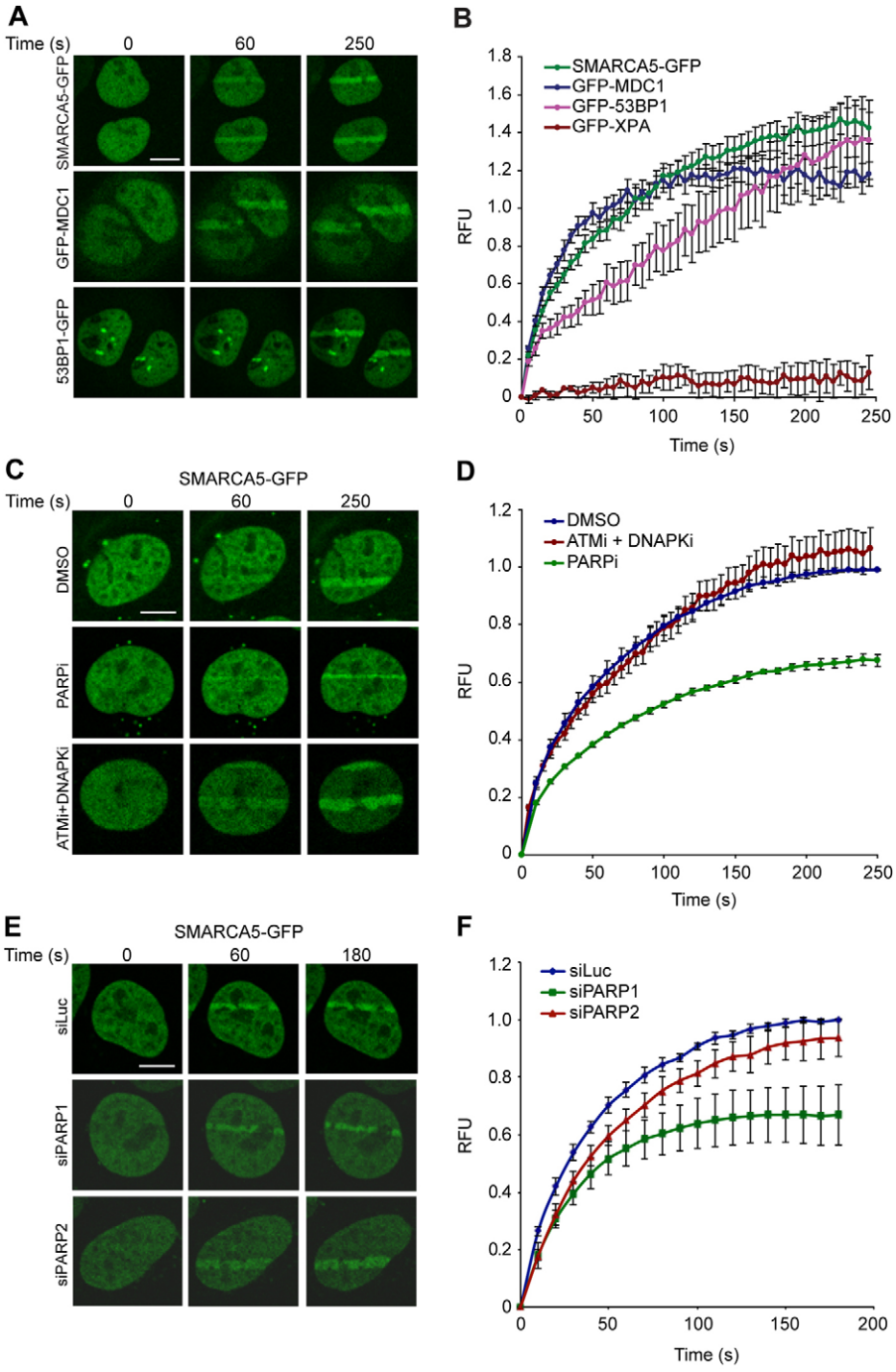

Fig. 2. SMARCA5 accumulation at sites of laser-induced DNA damage requires PARP. (**A**) U2OS cells expressing SMARCA5–GFP, GFP–MDC1, 53BP1–GFP or GFP–XPA were laser-irradiated and subjected to real-time recording of protein assembly at the damaged area. (GFP–XPA images not shown.) (**B**) Quantitative representation of results in A. Relative fluorescence units (RFU) are plotted against time. Values are means ± s.e.m. of at least 10 individual cells from independent experiments. (**C**) As in A, except that U2OS cells expressing SMARCA5–GFP were treated with inhibitors of PARP or ATM and DNA-PK. (**D**) Quantitative representation of results in C. (**E**) As in C, except that cells were transfected with siRNAs against PARP1 or PARP2. (**F**) Quantitative representation of results in E. Scale bars: 10 μm.

itself and acceptor proteins, directs the recruitment of the chromatin remodeling enzymes ALC1 and CHD4 to DSBs (Ahel et al., 2009; Chou et al., 2010; Gottschalk et al., 2009; Luijsterburg et al., 2012a; Polo et al., 2010). These findings prompted us to test the involvement of PARP enzymes in the recruitment of SMARCA5 to DSBs. Interestingly, SMARCA5 accumulation in DSB-tracks was significantly reduced, but not abolished, whereas ALC1 accumulation was abrogated in cells treated with PARPi (Fig. 2C,D; supplementary material Fig. S5A). Moreover, depletion of PARP1, but not PARP2, reduced SMARCA5 recruitment to similar levels as treatment with PARPi (Fig. 2E,F). These results implicate the catalytic activity of PARP1 in SMARCA5 recruitment to DNA strand breaks.

PARP regulates chromatin expansion and the distribution of SMARCA5 along damaged chromatin

When we examined the effect of PARP inhibition on SMARCA5 accumulation at DNA breaks, we noticed a reduction in the width of the SMARCA5-GFP-containing laser-tracks (Fig. 2C; Fig. 3C). This suggests that SMARCA5 fails to spread into the DSB-flanking chromatin compartment when PARP is inhibited. DNA damage induced by laser micro-irradiation triggers local chromatin expansion *in vivo* (Kruhlak et al., 2006), while

PARylation of nucleosomes triggers chromatin expansion *in vitro* (Poirier et al., 1982). We therefore tested whether PARP affects chromatin expansion at DNA damage sites and whether this event regulates the spreading of DSB response factors throughout damaged chromatin. In order to measure the extent of chromatin expansion in our experimental set-up, we expressed histone H2A fused to photoactivatable green fluorescent protein (PAGFP-H2A) (Patterson and Lippincott-Schwartz, 2002), to simultaneously inflict localized DNA damage and activate PAGFP-H2A only in the damaged chromatin compartment after multiphoton excitation. Indeed, PAGFP-H2A was activated immediately following DNA damage induction after which

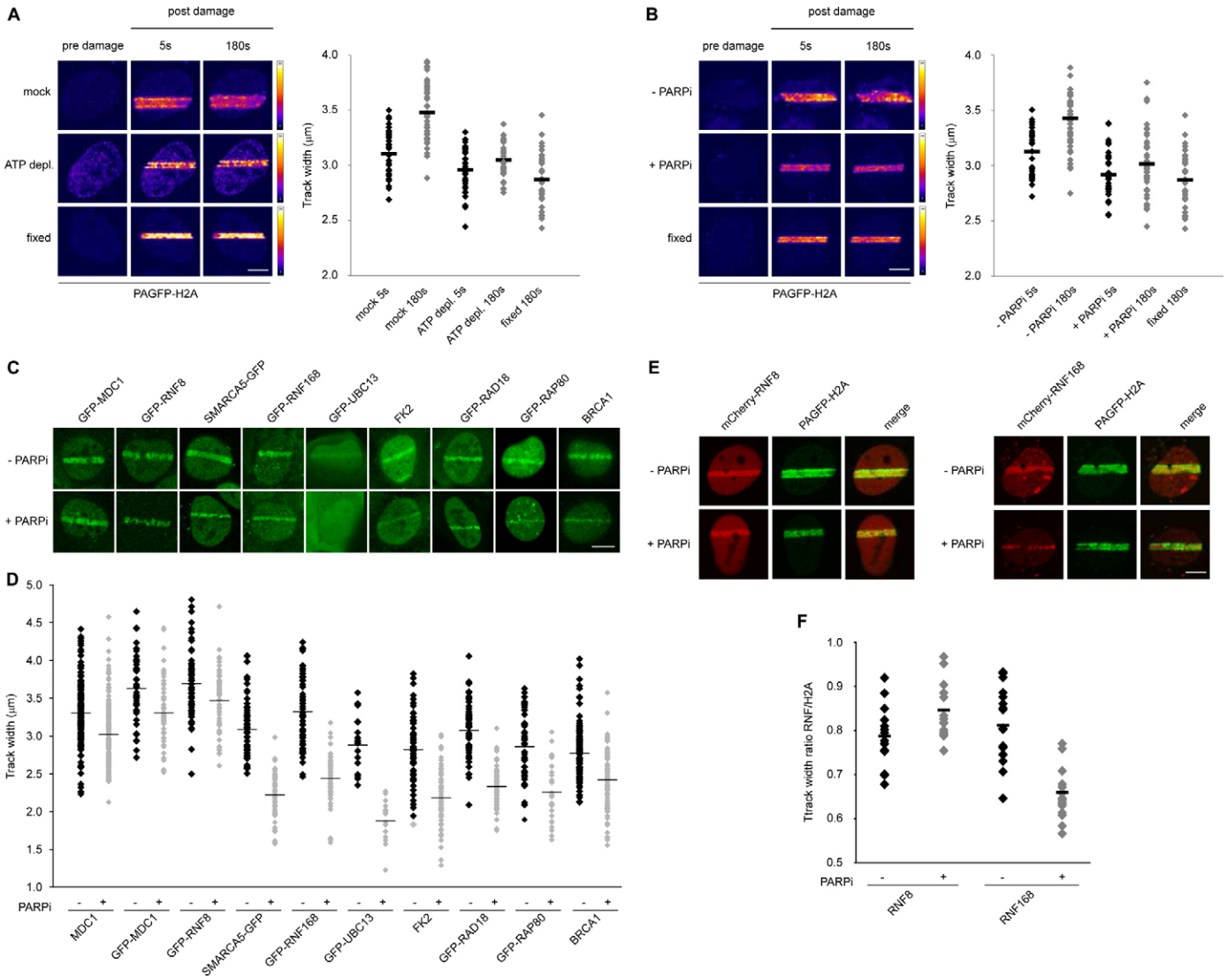

Fig. 3. PARP distributes SMARCA5 and factors of the RNF168 cascade throughout damaged chromatin. (**A**) U2OS cells expressing PAGFP-H2A were locally irradiated with a multiphoton laser to simultaneously photoactivate PAGFP and inflict DNA damage. Cells were cultured in mock or ATP-depletion medium, or chemically fixed in 4% formaldehyde prior to photoactivation. Images were recorded at the indicated times. The recorded 8-bit grayscale images were converted into colored images using a look-up table based on pixel intensities in the grayscale image. The look-up table shown next to the images utilizes colors ranging from black to white representing pixel intensities ranging from 0 (black) to 256 (white). Quantification of the expansion of the photoactivated chromatin compartment is shown next to the images. Scale bar: 5 μm. (**B**) As in A, except that cells were untreated or treated with PARPi. (**C**) Cells were left untreated or treated with PARPi, then subjected to multi-photon laser irradiation and analyzed for the expansion of the indicated GFP-fusion proteins or immunostained endogenous proteins throughout the damaged compartment. Representative images illustrating the effect of PARP inhibition on the expansion of the indicated proteins are shown. Scale bar: 10 μm. (**D**) Quantitative analysis of the width of laser-tracks from cells in C. Laser-tracks with a width of 1.5 μm were generated. After 180 s the width of the region showing accumulation of the indicated proteins was measured to determine the increase in track width. Individual measurements ($n \geq 16$) and mean values are presented in a track-width distribution plot. (**E**) Cells were co-transfected with PAGFP-H2A and either mCherry-RNF8 or mCherry-RNF168 to simultaneously monitor chromatin expansion and spreading of mCherry-tagged RNF8 or RNF168 in the same track. Cells were untreated or treated with PARPi, irradiated with the multiphoton laser and images were recorded in two channels. Scale bar: 5 μm. (**F**) Quantitative analysis of mCherry–RNF8 and mCherry-RNF168 spreading in cells from E. The track width for these proteins was normalized to that of PAGFP-H2A in the same cells for each of the indicated conditions.

PAGFP-H2A tracks rapidly expanded within the first 3 minutes following irradiation (Fig. 3A,B). The observed expansion is a biological phenomenon as it was inhibited by depletion of ATP and abolished in chemically fixed cells (Fig. 3A,B). Remarkably, treatment with PARPi suppressed the DNA damage-induced expansion of chromatin similar to ATP depletion, highlighting a novel role for the synthesis of poly(ADP-ribose) chains in this process (Fig. 3B). These findings implicate PARP activity in chromatin expansion at sites of DNA damage.

PARP regulates the distribution of factors of the RNF168 cascade along damaged chromatin

Having observed that PARPi affects chromatin expansion and SMARCA5 spreading into damaged chromatin (Fig. 2C; Fig. 3C), we decided to determine its effect on the expansion of other DSB response factors. In control cells we could detect rapidly expanding accumulation of GFP-tagged MDC1, RNF8, RNF168 and SMARCA5 at laser-tracks, indicative of efficient spreading into damaged chromatin (Fig. 3C,D; supplementary material Fig. S5B). Strikingly, PARP inhibition reduced the spreading of GFP-MDC1 and that of its binding partner GFP-RNF8 in these tracks to a similar extent as observed for PAGFP-H2A (Fig. 3B–D; supplementary material Fig. S5B). Since MDC1 and RNF8 physically associate with γH2AX (Huen et al., 2007; Kolas et al., 2007; Mailand et al., 2007; Stucki et al., 2005), a constituent of damaged chromatin, our results suggest that the reduced distribution of MDC1 and RNF8 is a direct consequence of impaired chromatin expansion caused by inhibiting PAR synthesis. Conversely, SMARCA5-GFP distribution along laser-tracks was impaired by PARPi to a greater extent than PAGFP-H2A (Fig. 3B–D; supplementary material Fig. S5B). A similar impact on track width was measured using a low PARPi concentration that inhibits PARP1 rather than PARP2 (Boehler et al., 2011), or when PARP1, but not PARP2, was depleted (supplementary material Fig. S6). This indicates that PARP1 is required for efficient spreading of SMARCA5 into damaged chromatin. Consistent with a selective effect on SMARCA5, we found that laser-tracks marked by SMARCA5-GFP showed little expansion in the presence of PARPi, while the spreading of endogenous MDC1 along the same tracks was much more pronounced (supplementary material Fig. S5C), albeit reduced compared to the spreading of MDC1 in control cells. Surprisingly, while PARPi did not affect RNF8 expansion beyond the impaired chromatin expansion, we found that GFP-RNF168 spreading was impaired in response to PARP inhibition to the same extent as SMARCA5 (Fig. 3C,D; supplementary material Fig. S5B). Consequently, we found that the distribution of GFP-UBC13 and conjugated ubiquitin along DSB-containing chromatin was also significantly impaired after PARP inhibition (Fig. 3C,D). Ubiquitin conjugates generated by RNF8 and RNF168 mediate recruitment of ubiquitin-binding factors RAD18 and the RAP80–BRCA1 complex (Huang et al., 2009; Kim et al., 2007; Sobhian et al., 2007; Wang et al., 2007). Consistent with the defective spreading of ubiquitin conjugates, we found that PARPi also significantly reduced the expansion of GFP-RAD18, GFP-RAP80 and endogenous BRCA1 (Fig. 3C,D).

Taken together, our analysis suggests that PAR synthesis regulates the spatial organization of the DDR in two distinct ways. Firstly, PARP activity promotes efficient expansion of damaged chromatin occupied by MDC1 and RNF8. Secondly, PARP activity orchestrates the spreading of SMARCA5, RNF168 and downstream factors into damaged chromatin. To directly distinguish between these events we expressed mCherry-RNF8 or mCherry-RNF168 in cells together with PAGFP-H2A, allowing us to simultaneously measure expansion of H2A and spreading of mCherry-tagged ubiquitin ligases along damaged chromatin. This analysis confirmed that the reduced spreading of RNF8 in PARPi-treated cells corresponds to reduced chromatin expansion in the same tracks, since the normalized spreading in control and PARP-inhibited cells was remarkably similar (Fig. 3E,F). Conversely, the normalized spreading of RNF168 in cells treated with PARPi was markedly reduced compared to control cells, showing that PARP inhibition uncouples the efficient spreading of DDR factors involved in the RNF168 response (Fig. 3E,F). Thus, our findings uncover unanticipated PARP-driven mechanisms that regulate the DNA damage-induced expansion of chromatin and the occupancy of SMARCA5 and factors of the RNF168 signaling cascade throughout damaged chromatin.

SMARCA5 and RNF168 interact in a DNA damage- and PARP-dependent manner

The fact that PARP1 regulates the distribution of both SMARCA5 and factors of the RNF168 signaling cascade suggests a functional link between SMARCA5 chromatin remodeling and RNF168-dependent signaling of DSBs. To gain mechanistic insight into these events, we considered the possibility that SMARCA5 may interact with RNF168. To test this hypothesis, we screened the RNF168 interactome by quantitative mass spectrometry. This approach revealed an interaction between RNF168 and SMARCA5 after exposure of cells to IR, but not to UV-C light (Fig. 4A). Immunoprecipitation followed by western blot analysis confirmed the IR-dependent interaction between endogenous RNF168 and SMARCA5 (Fig. 4B). Furthermore, we demonstrated that streptavidin-tagged RNF168 interacts with endogenous SMARCA5 and showed in the reciprocal experiment that GFP-tagged SMARCA5 associates with endogenous RNF168 (Fig. 4C,D). Given that PARPi selectively affects the spreading of SMARCA5 and RNF168 into damaged chromatin, we investigated whether PARP inhibition affects the interaction between SMARCA5 and RNF168. Remarkably, we found that, although treatment with PARPi slightly enhanced the interaction in non-irradiated cells, it nearly abrogated the IR-induced interaction between endogenous SMARCA5 and RNF168 (Fig. 4E).

RNF168 is a DNA damage-dependent substrate of poly(ADP-ribosyl)ation

PARP1 not only targets itself for PARylation, but also several other non-histone and histone proteins involved in the DSB response (Messner and Hottiger, 2011). We therefore examined whether the PARP-dependent interaction between SMARCA5 and RNF168 may involve PARylation of either of these proteins. We exposed cells to IR or the DNA alkylating agent MNNG and compared the PARylation status of SMARCA5 and RNF168 to that of PARP1. In whole cell extracts (WCE), we observed a significant increase in PARylated proteins after MNNG treatment, and a moderate increase shortly after exposure to IR (Fig. 4F), indicating that these treatments result in activation of PARP enzymes. We subsequently immunoprecipitated GFP-tagged PARP1, SMARCA5 or RNF168 from untreated, IR-treated or MMNG-treated cells

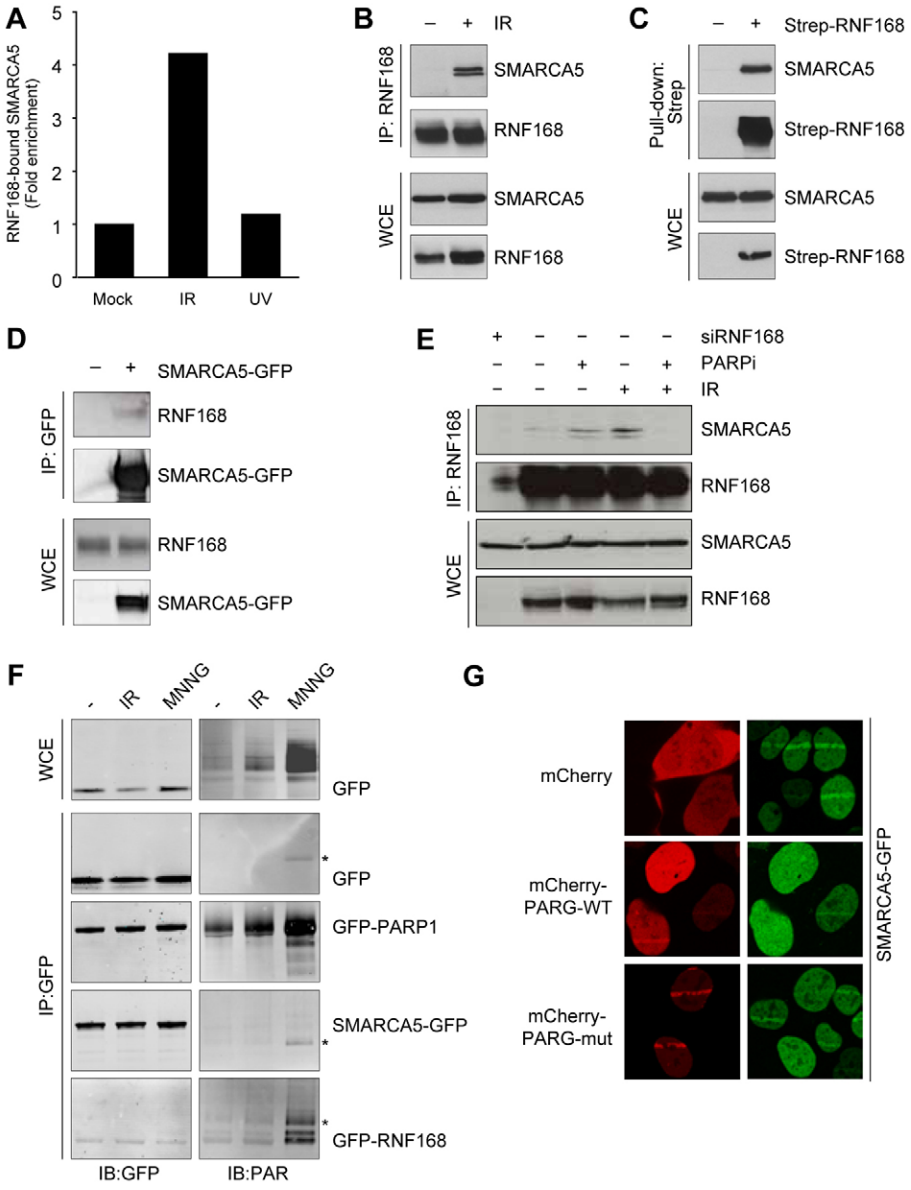

Fig. 4. SMARCA5 interacts with RNF168 in a PARP-dependent manner. (**A**) U2OS cells were SILAC-labeled for 7 days and then mock-treated or exposed to 10 Gy IR or 25 J/m^2 UV. 1 h later, cells were harvested and subjected to RNF168 immunoprecipitation (IP). Bound complexes were washed, eluted and analyzed by mass spectrometry. SILAC ratios measured for the SMARCA5–RNF168 interaction (defined as 1 in the mock sample) are shown. (**B**) HeLa cells were mock-treated or exposed to 10 Gy IR and harvested 1 h later. Whole cell extracts (WCE) were subjected to RNF168 IP followed by immunoblotting for the indicated proteins. (**C**) HEK293T cells were transfected with Strep-RNF168 plasmid or empty vector and harvested 24 h later. Cell extracts were incubated with Strep-Tactin Sepharose and bound complexes were analyzed by immunoblotting for the indicated proteins. (**D**) HEK293T cells were transfected with SMARCA5-GFP plasmid or empty vector and harvested 24 h later. Cell extracts were subjected to GFP IP followed by immunoblotting for the indicated proteins. (**E**) As in B, except that cells were treated with siRNA against RNF168 or PARPi. (**F**) U2OS cells were transfected with GPP, GFP-PARP1, SMARCA5-GFP or RNF168-GFP plasmid, and 24 h later mock-treated or exposed to 10 Gy IR or 100 µM MNNG for 5 minutes and harvested. WCE were prepared in the presence of PARG inhibitor and subjected to GFP immunoprecipitation (IP). Bound GFP proteins were washed using high salt conditions to disrupt protein complexes, then eluted and examined by immunoblotting for GFP and PAR. Non-specific bands are indicated with an asterisk. PAR signals were normalized to those of GFP. The ratio for treated cells was normalized to that for untreated cells, which was set to 1. PARylation levels were increased in WCE after IR (2- to 3-fold) and MNNG (8-fold) treatment. PARylation of PARP1 was increased after MNNG (2- to 3-fold), while PARylation of RNF168 was increased after both IR and MNNG (2- to 3-fold and 9-fold, respectively). (**G**) U2OS cells expressing SMARCA5-GFP were transfected with mCherry, mCherry-PARG-WT or mCherry-PARG-mut plasmid, 24 h later subjected to multi-photon laser-irradiation and analyzed for protein accumulation in the irradiated region. Representative images illustrating the inhibitory effect of PARG-WT and PARG-mut expression on the accumulation of SMARCA5 in DSB-tracks are shown.

and examined the PARylation status of these proteins by western blot analysis. As expected, PARP1 was robustly PARylated upon IR or MNNG exposure (Fig. 4F), showing that our approach can detect the attachment of PAR chains to proteins in response to genotoxic stress. Surprisingly, RNF168 was also a substrate of PARylation following IR and MNNG

treatment (Fig. 4F). The stronger PARylation of RNF168 after MNNG treatment closely mirrored the induction of PAR synthesis in WCE, most likely reflecting the more robust activation of PARP1 after MNNG. Nonetheless, following IR, we detected a reproducible increase in PARylated RNF168 compared to non-irradiated cells. Conversely, we failed to detect DNA damage-induced PARylation of SMARCA5, suggesting that this protein is not modified by PARP following DNA damage induction. Thus, we identify RNF168 as a new DNA damage-induced substrate of poly(ADP-ribosyl)ation.

PAR chains are required for SMARCA5 accumulation at sites of DNA damage

A large-scale proteomics analysis identified SMARCA5 as a putative PAR-binding protein (Gagné et al., 2008). To investigate the relevance of this observation for the DSB response, we explored the *in vivo* interaction between SMARCA5 and PAR following DNA damage induction. If SMARCA5 binds PAR chains, we would expect that modulating the transient nature of these structures affects SMARCA5 accumulation at DSBs. We therefore expressed either wild-type or catalytically inactive mCherry-tagged isoforms of poly(ADP-ribose) glycohydrolase (PARG), the enzyme that hydrolyzes PAR chains, in cells expressing SMARCA5–GFP and studied their effect on SMARCA5 accumulation in DSB-tracks. Overexpression of mCherry alone did not affect SMARCA5 accumulation at DSB-tracks (Fig. 4G). However, overexpression of wild-type PARG (PARG-WT), which results in reduced steady-state levels of PAR chains at damaged sites (Ismail et al., 2012), strongly impaired SMARCA5 accumulation (Fig. 4G). In addition, overexpression of catalytically inactive PARG (PARG-mut), which does not affect the steady-state levels of PAR chains, but efficiently blocks PAR chain accessibility by binding to these structures (Ismail et al., 2012), abrogated SMARCA5 recruitment (Fig. 4G). Thus, lowering the availability of PAR chains by PARPi, PARP1 knockdown or overexpression of PARG-WT or PARG-mut considerably reduces the recruitment of SMARCA5 (Fig. 2C–F; Fig. 4G). These findings provide *in vivo* evidence suggesting that SMARCA5 requires the synthesis of PAR chains for its recruitment to sites of DNA damage, where it directly binds these structures. Given that RNF168 is a novel DNA damage-dependent substrate of PARylation, a scenario emerges in which SMARCA5 binds to PAR chains present on RNF168 at sites of DNA damage.

SMARCA5 and RNF168 accumulation at DSBs is mutually dependent

The interaction between SMARCA5 and RNF168 raises the question whether SMARCA5 is required for an efficient RNF168-ubiquitin response to DNA damage. To this end, we examined the impact of SMARCA5 depletion on IRIF formation of several factors involved in the RNF168 cascade. We found that SMARCA5 knockdown affected neither γH2AX and MDC1, nor RNF8 accumulation into IRIF (Fig. 5A,B). In agreement, western blot analysis showed normal IR-induced γH2AX levels in these cells (supplementary material Fig. S8A). This suggests that SMARCA5 does not affect the early stages of the DSB response. In contrast, accumulation of RNF168 into IRIF was severely impaired by SMARCA5 depletion (Fig. 6A,B). Corroborating these findings, GFP-RNF168 accumulation in laser-tracks was also markedly impaired by SMARCA5 depletion (Fig. 6C,D). Conversely, we found that RNF168 knockdown reduced SMARCA5-GFP assembly in DSB-tracks (Fig. 6E,F). The finding that SMARCA5 and RNF168 accumulation is mutually dependent is in line with the PARP-dependent expansion of these proteins throughout damaged chromatin and their physical, PARP-dependent interaction in response to DNA damage.

SMARCA5 stimulates γH2AX ubiquitylation and BRCA1 accumulation at DSBs

In agreement with impaired RNF168 recruitment, we then found that ubiquitin conjugation in IRIF was also substantially reduced in SMARCA5-depleted cells (Fig. 7A,B). Given that H2A and H2AX are the primary known targets for IR-induced

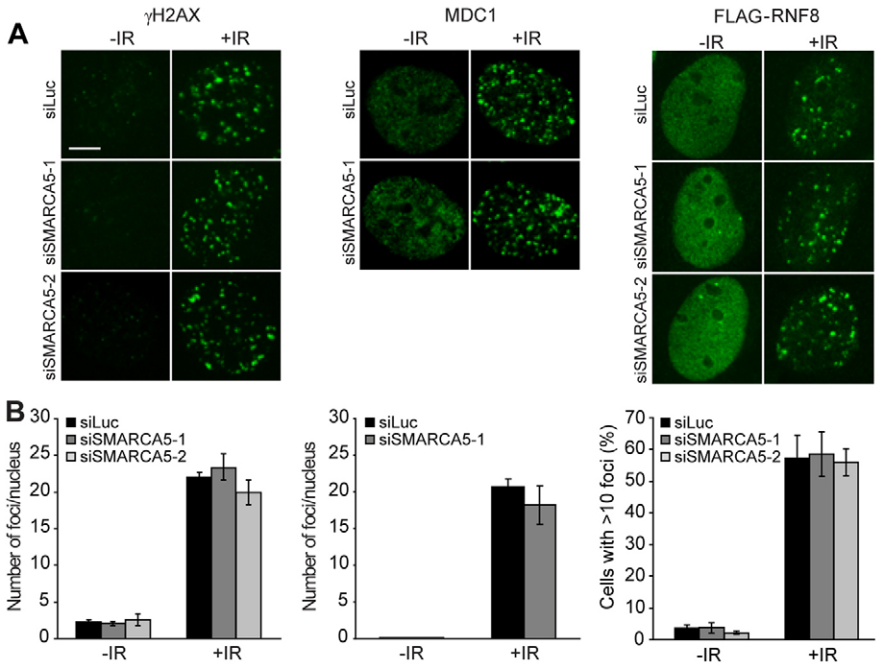

Fig. 5. SMARCA5 does not promote γH2AX, MDC1 or RNF8 accumulation at DSBs. (**A**) U2OS cells or doxycycline-treated U2OS cells expressing FLAG-RNF8 and an shRNA against RNF8 were transfected with the indicated siRNAs, exposed to 1 Gy IR and 1 h later immunostained for γH2AX, MDC1 or FLAG-RNF8 to visualize IRIF (Mailand et al., 2007). Scale bar: 10 µm. (**B**) Quantitative representation of γH2AX (left), MDC1 (middle) or FLAG-RNF8 (right) IRIF formation in A. The average number of foci/nucleus ± s.e.m. is presented for γH2AX and MDC1, whereas the percentage of cells with more than 10 foci ± s.e.m. is presented for FLAG-RNF8. More than 150 nuclei were scored per treatment in independent experiments.

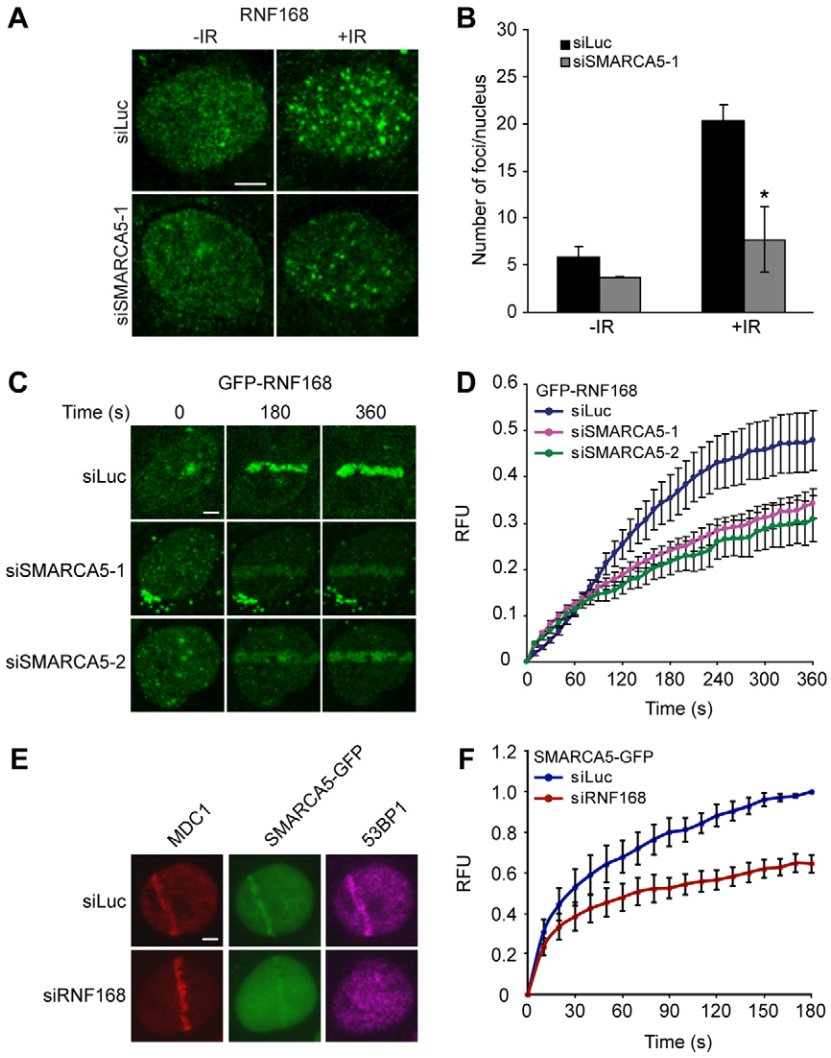

Fig. 6. SMARCA5 promotes RNF168 assembly at DSBs. (**A**) U2OS cells were transfected with the indicated siRNAs, exposed to 1 Gy IR and 1 h later immunostained for RNF168 to visualize IRIF. (**B**) Quantitative representation of RNF168 IRIF formation in A. The average number of foci/nucleus ± s.e.m. is presented. More than 150 nuclei were scored per treatment in independent experiments. *$P<0.05$, compared with siLuc (control). (**C**) U2OS cells expressing GFP-RNF168 were transfected with the indicated siRNAs, laser-irradiated and subjected to real-time recording of protein assembly at the damaged area. (**D**) Quantitative representation of results in C. Relative fluorescence units (RFU) are plotted against time. Values are means ± s.e.m. of at least 10 individual cells from independent experiments. (**E**) As in C, except that U2OS cells expressing SMARCA5-GFP were used and transfected with siRNAs against RNF168. (**F**) As in D, except that cells from E were analyzed. Scale bars: 5 µm.

ubiquitylation (Doil et al., 2009; Huen et al., 2007; Mailand et al., 2007; Stewart et al., 2009; Wang et al., 2007), we immunoprecipitated γH2AX from untreated and IR-exposed cells and examined its ubiquitylation status by western blot analysis. In agreement with our IRIF data, we found that SMARCA5 knockdown decreased IR-induced γH2AX mono- and di-ubiquitylation, similar to that observed after RNF8 or RNF168 knockdown (Fig. 7C,D) (Huen et al., 2007). As expected, SMARCA5 and RNF168 co-depletion did not reduce γH2AX ubiquitylation beyond that observed after depletion of the individual proteins, consistent with the notion that SMARCA5 operates in the RNF168-dependent ubiquitin cascade (data not shown).

We next analyzed recruitment of the RAP80–BRCA1 complex, which binds to conjugated ubiquitin for its accumulation at DSBs (Sobhian et al., 2007; Wu et al., 2009). Consistent with the defects in ubiquitin conjugation, we found that BRCA1 recruitment into IRIF was impaired in SMARCA5-depleted cells (Fig. 7E,F) (Nakamura et al., 2011). Surprisingly however, we did not observe any defect in 53BP1 IRIF formation in SMARCA5-depleted cells, even though ubiquitin conjugation and BRCA1 assembly were significantly impaired in the same cells (supplementary material Fig. S7). As expected, depletion of RNF8 not only impaired ubiquitin conjugation, but also 53BP1 accumulation in IRIF (Huen et al., 2007; Kolas et al., 2007; Mailand et al., 2007) (supplementary material Fig. S7A,B). This suggests that the threshold for ubiquitin levels required to promote either BRCA1 or 53BP1 recruitment may differ, or that alternative mechanisms exist that promote 53BP1 accumulation at damage sites when the SMARCA5-RNF168 response is impaired.

Finally, we assessed whether the ATPase activity of SMARCA5, essential for its chromatin remodeling activity, is required for BRCA1 accumulation. We expressed GFP-tagged wild-type SMARCA5 or ATPase-dead SMARCA5-K211R in cells depleted of endogenous SMARCA5 (Lan et al., 2010). As shown before, SMARCA5 depletion severely impaired BRCA1 recruitment into IRIF (Fig. 8A–C). This defect was fully rescued by exogenous expression of wild-type SMARCA5 (Fig. 8A–C). Conversely, expression of ATPase-dead SMARCA5 failed to rescue this defect (Fig. 8A–C), suggesting that the ATPase activity of SMARCA5 is essential for BRCA1 accumulation at DSBs.

Discussion

Our study revealed that SMARCA5 protects cells against IR and regulates the two major pathways of DSB repair, HR and

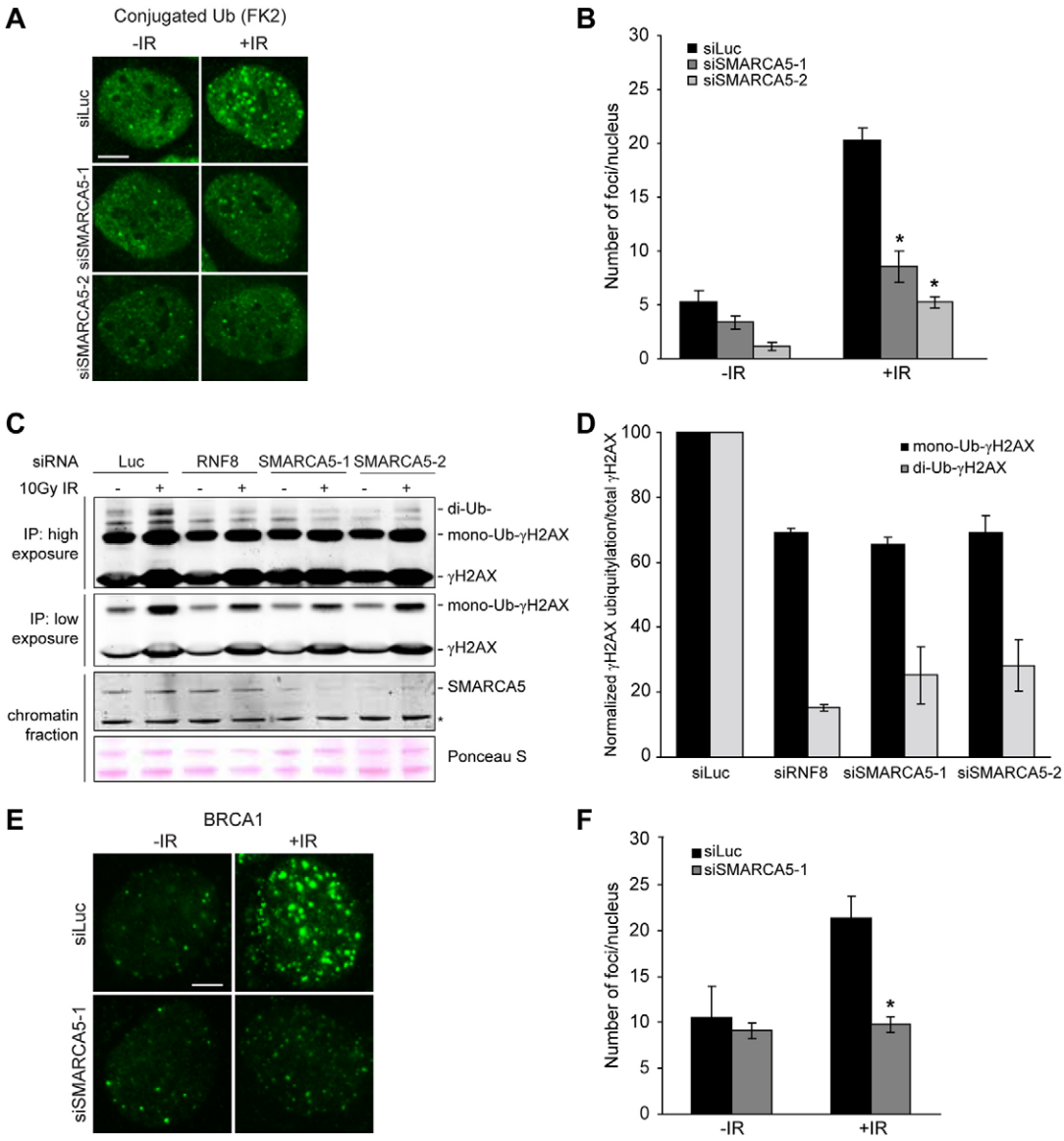

Fig. 7. SMARCA5 promotes γH2AX ubiquitylation and BRCA1 accumulation at DSBs. (**A**) Cells were transfected with the indicated siRNAs, exposed to 1 Gy IR and 1 h later immunostained for conjugated ubiquitin (FK2) to visualize IRIF. Scale bar: 10 μm. (**B**) Quantitative representation of FK2 IRIF formation in A. The average number of foci/nucleus ± s.e.m. is presented. More than 150 nuclei were scored per treatment in independent experiments. *$P<0.05$, compared with siLuc (control). (**C**) Cells transfected with the indicated siRNAs were exposed to 10 Gy IR. 1 h later chromatin-enriched extracts (CEE) were prepared. CEE were subjected to IP with γH2AX antibody. Western blot analysis of IP with γH2AX antibody, and CEE with SMARCA5 antibody are shown. Ponceau S staining was used as a loading control. (**D**) Graphical representation of relative γH2AX ubiquitylation levels determined using results from C. Ratios of unmodified γH2AX and either mono-ubiquitylated or di-ubiquitylated γH2AX were normalized to that of control cells, which was set to 1. The means ± s.e.m. of two independent experiments is shown. (**E**) As in A, except that cells were immunostained for BRCA1. (**F**) As in B, except that cells from E were analyzed.

NHEJ, which is in line with two recent reports (Lan et al., 2010; Nakamura et al., 2011). In addition, we uncover an unrecognized role of SMARCA5 in regulating the RNF168 signaling cascade at DSBs. SMARCA5 and RNF168 interact in the DSB-flanking chromatin compartment in a PARP-dependent manner to regulate RNF168-dependent histone ubiquitylation and subsequent BRCA1 assembly, which requires SMARCA5 ATPase activity. Our findings unveil a novel physical and functional link between DNA damage-induced PARylation, chromatin remodeling and the RNF8/RNF168-signaling cascade (Fig. 8D).

SMARCA5 protects against DNA damage

ISW-1 was identified through a genetic screen in *C. elegans* as a factor that protects worms against IR (van Haaften et al., 2006). We provide evidence that one of its human orthologues, SMARCA5, also protects cells against the genotoxic effects of IR. SMARCA5-depleted cells displayed hypersensitivity to IR, indicating that the DSB response may be compromised. This could indirectly stem from altered gene expression in response to IR. However, we found that loss of SMARCA5 did not affect steady-state levels of key DDR factors (MDC1, RNF8, RNF168, 53BP1, BRCA1, BRCA2, RAD51 and p53), either before or after

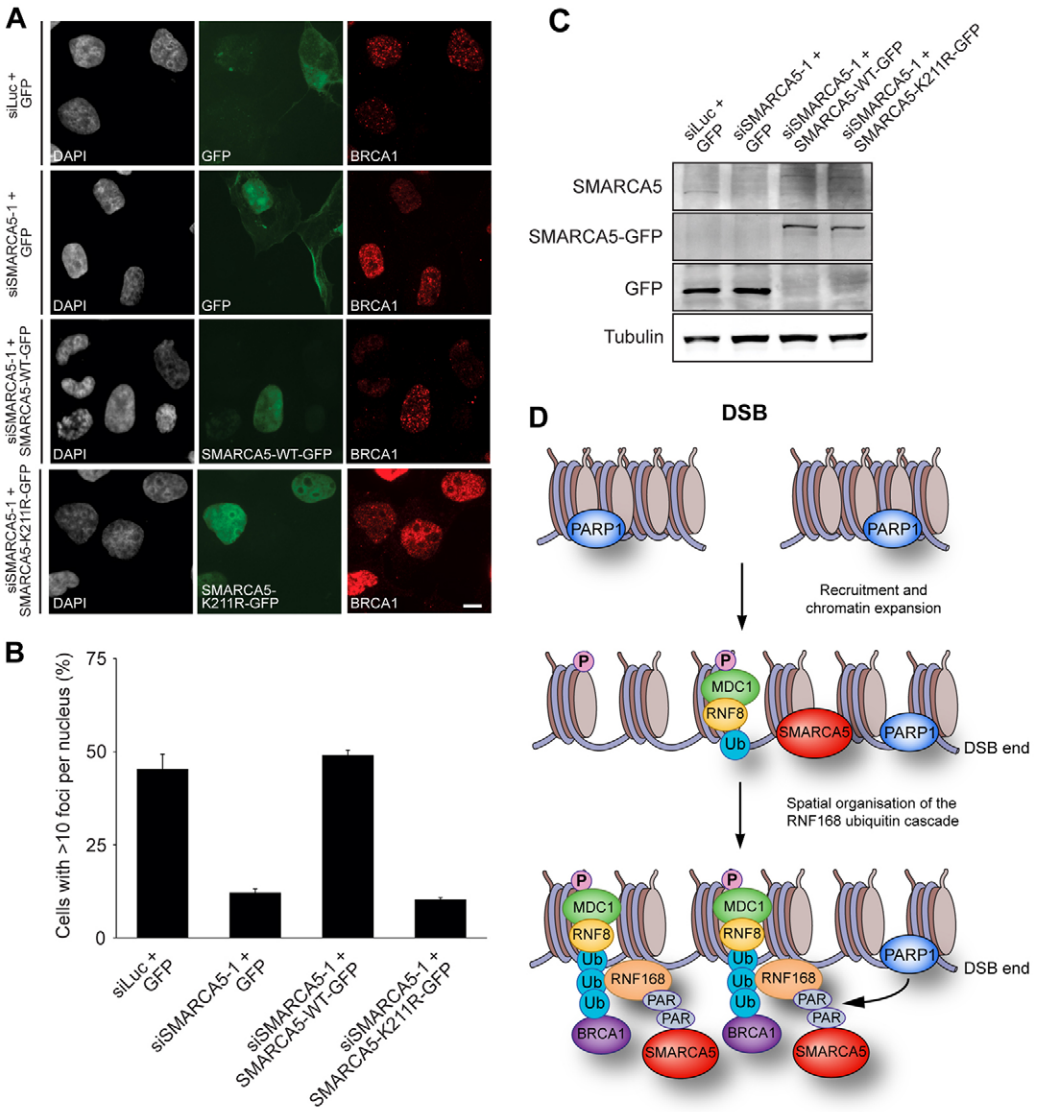

Fig. 8. SMARCA5 chromatin remodeling activity is required for BRCA1 accumulation at DSBs. (**A**) U2OS cells were transfected with the indicated siRNAs and either GFP, SMARCA5-WT-GFP or SMARCA5-K211R-GFP plasmids, exposed to 2 Gy IR and stained for BRCA1 and DAPI. Scale bar: 5 μm (**B**) Quantitative representation of BRCA1 IRIF formation in A. The percentage of cells with more than 10 foci per nucleus is presented. Error bars indicate the s.d. More than 100 cells from at least two independent experiments were scored. (**C**) SMARCA5 and SMARCA5-GFP levels were monitored by western blot analysis using whole cell extracts of cells in A. Tubulin was used as a loading control. (**D**) Model for the role of SMARCA5 in the DSB response. A DSB in chromatin triggers PARP1 recruitment and γH2AX formation. PARP1 elicits local chromatin expansion, whereas γH2AX promotes the accumulation of MDC1 and RNF8, which ubiquitylates H2A-type histones. This leads to RNF168 recruitment, which amplifies RNF8-induced ubiquitylation, promoting the accumulation of ubiquitin-binding factors, including the RAP80–BRCA1 complex. PARP1 promotes the spatial distribution of SMARCA5 and factors of the RNF168 signaling cascade (RNF168, UBC13, RAD18, RAP80, BRCA1; only RNF168 and BRCA1 are shown for simplicity), and stimulates SMARCA5 and RNF168 interaction throughout DSB-flanking chromatin, most likely through PARylation of RNF168, thereby regulating RNF168-dependent DSB signaling. SMARCA5 also promotes efficient repair of DSB by NHEJ and HR (see text for details).

exposure of cells to IR (supplementary material Fig. S8), suggesting that SMARCA5 protects human cells against IR by acting directly at DSBs to promote DSB repair. Consistently, we and others have shown that SMARCA5 is recruited to DSBs where it regulates DSB repair by both HR and NHEJ (Lan et al., 2010; Nakamura et al., 2011).

PARP and the recruitment of SMARCA5 to DSBs

SMARCA5 is recruited to both site-specific chromosomal DSBs induced by the I-*Sce*I or A*si*SI nucleases and to laser-induced DNA damage (Fig. 1F; supplementary material Fig. S3C,D) (Erdel et al., 2010; Lan et al., 2010; Nakada et al., 2010; Sánchez-Molina et al., 2011). Nakamura and co-workers implicated a role for the RNF20 E3 ubiquitin ligase in SMARCA5 recruitment to DNA breaks (Nakamura et al., 2011), whereas, another report suggested a role for ACF1 in SMARCA5 recruitment to DSBs, although formally it was not shown that ACF1 loss abrogates SMARCA5 assembly at DSBs (Lan et al., 2010). We extend these findings by demonstrating that SMARCA5 is rapidly recruited to DSBs in a manner that

requires the activity of PARP1 (Fig. 2). Given that RNF20 and potentially ACF1 also contribute to SMARCA5 assembly at DNA strand breaks (Lan et al., 2010; Nakada et al., 2010), it will be of interest to unravel how the crosstalk between PARP1, RNF20 and ACF1 activities orchestrates SMARCA5 accumulation and/or activity at DSB sites.

How does PARP1 activity affect SMARCA5 accumulation at DSB sites? It is known that PARP1 not only targets itself for PARylation, but also several other non-histone and histone proteins involved in the DSB response (Messner and Hottiger, 2011). Two chromatin remodeling enzymes, ALC1 and CHD4, contain PAR-binding regions and require PARP activity for their efficient recruitment to DNA damage sites (Ahel et al., 2009; Chou et al., 2010; Gottschalk et al., 2009; Polo et al., 2010). Interestingly, we identified RNF168 as a novel substrate for DNA damage-induced PARylation, and obtained *in vivo* evidence suggesting that SMARCA5 binds to PAR chains, potentially those on RNF168. Consistent with this, we found that SMARCA5 and RNF168 interact in a DNA damage- and PARP-dependent manner. However, precisely how SMARCA5 interacts with PARylated RNF168 is not yet clear. SMARCA5 does not contain a canonical macro-domain or PBZ zinc finger domain for PAR binding. It harbors a putative PAR-binding sequence, but a recent report demonstrated that this sequence was dispensable for PAR binding *in vitro* (Gagné et al., 2008), suggesting that it may not be required for SMARCA5 accumulation at DSBs. In line with this, mutation of the putative PAR binding sequence indicated that it is dispensable for PARP-dependent accumulation of SMARCA5 in DSB-tracks (supplementary material Fig. S9). This suggests that other regions in SMARCA5 may be responsible for the association with PARylated proteins such as RNF168, and spreading within the damaged chromatin compartment. Alternatively, one of the many binding partners of SMARCA5 may contain a PAR-binding sequence and associate with PARylated proteins such as RNF168 at sites of DNA damage, contributing to SMARCA5 accumulation at DNA damage sites.

PARP links SMARCA5 to the RNF168 signaling cascade at DSBs

The rapid recruitment of PARP1 to DNA strand breaks is in line with its role in the rapid recruitment of SMARCA5 to DSBs (Haince et al., 2008). Given that PARP1 contributes to SMARCA5 recruitment and SMARCA5 regulates efficient RNF168 and BRCA1 assembly at DSBs, our work suggests that PARP1 modulates the RNF168-dependent ubiquitylation response, which elicits BRCA1 accumulation at DNA breaks.

Previous work suggested that laser micro-irradiation evokes chromatin expansion independently of ATM or γH2AX (Kruhlak et al., 2006). We showed that PARP is involved in this process as PARP inhibition moderately reduces chromatin expansion at sites of laser-induced DNA damage (Fig. 3). In addition, we found PARP inhibition to selectively impair SMARCA5 distribution, as well as that of RNF168 and several of its downstream factors, into DSB-flanking chromatin regions (Fig. 3; supplementary material Fig. S5B,C). This suggests that PARP affects the distribution of a specific subset of RNF168-associated factors into damaged chromatin regions, while it is dispensable for the spreading of other factors, such as RNF8 and MDC1. Given that SMARCA5 recruitment to DSBs is partially PARP1-dependent and considering that SMARCA5 interacts with RNF168 in damaged chromatin in a PARP-dependent manner, it is tempting to speculate that SMARCA5 is required for the spreading of repair and signaling factors of the RNF168 response. It may be that the correct distribution of these factors is important for their sustained retention at DSBs. In support of this, we found that SMARCA5 loss affects the accumulation of RNF168, ubiquitin and BRCA1 at DSBs, but not that of MDC1 and RNF8 (Figs 5–7). Thus, our work demonstrates that the interplay between PARP activity, SMARCA5 chromatin remodeling and RNF168 ubiquitylation plays an important role in the DSB response. We propose a model in which SMARCA5 and RNF168 are recruited to DSBs through pathways involving PARP1 and ATM/γH2AX/MDC1/RNF8, respectively (Fig. 8) (Doil et al., 2009; Stewart et al., 2009). Once recruited, PARP1 not only promotes the redistribution of SMARCA5 and factors of the RNF168 cascade, but also stimulates the interaction between SMARCA5 and RNF168, which promotes ubiquitin conjugation, and the subsequent accumulation of BRCA1 in DSB-flanking chromatin (Fig. 8D).

Surprisingly, while PARP inhibition abrogated the IR-induced interaction between SMARCA5 and RNF168, it enhanced this interaction in non-irradiated cells. It seems unlikely that the interaction between these factors in non-irradiated cells is a consequence of DSB formation upon treatment with PARPi, given that the IR-induced SMARCA5–RNF168 interaction strictly requires PARP activity. Rather, in addition to the DNA damage-dependent interaction reported here, SMARCA5 and RNF168 may be indirect interaction partners in another multi-subunit protein complex. Given that PARP enzymes regulate many different processes, including transcription, mitosis and apoptosis (Kim et al., 2005), it may be that the SMARCA5-RNF168 interaction observed after PARP inhibition may be important for cellular homeostasis when PARP-mediated processes are perturbed. Nonetheless, the DNA damage-dependent interaction between these factors is strictly dependent on PARP activity and likely involves binding of SMARCA5 to PARylated RNF168 (Fig. 4).

SMARCA5 and other chromatin remodelers involved in the RNF168 cascade

In addition to SMARCA5 reported here, we have recently shown that CHD4 affects BRCA1 accumulation by promoting the ubiquitin signaling cascade at the level of RNF8/RNF168 (Larsen et al., 2010; Luijsterburg et al., 2012a; Smeenk et al., 2010). Likewise, p400, which is the catalytic subunit of the NuA4 complex, is another chromatin remodeling factor that has been shown to promote RNF8/RNF168-dependent ubiquitylation and BRCA1 assembly at DSBs (Doyon and Côté, 2004; Xu et al., 2010). Thus, three distinct chromatin remodeling factors play a role in BRCA1 assembly at DSBs. Mechanistically, it was shown that p400 forms a complex with MDC1 and its recruitment to DSBs requires MDC1 (Xu et al., 2010). Similarly, CHD4 directly binds to RNF8 and is recruited to DSB-containing tracks in a PARP- and RNF8-dependent manner (Luijsterburg et al., 2012a; Polo et al., 2010). We extend these findings by showing that SMARCA5 directly interacts with RNF168 in a PARP- and DNA damage-dependent manner and that SMARCA5 and RNF168 are recruited to DSBs in a mutually dependent manner. Thus, MDC1, RNF8 and RNF168, which are all involved in the ubiquitin response that promotes BRCA1 accumulation, recruit different chromatin remodeling enzymes to DSBs. These findings suggest that a consecutive series of distinct chromatin configurations

need to be established at DSBs when MDC1, RNF8 and RNF168 act at these sites to promote BRCA1 assembly (Luijsterburg and van Attikum, 2012). However, it remains to be established how CHD4, p400 and SMARCA5 remodel chromatin in the vicinity of DSBs to promote the RNF8/RNF168 signaling cascade. Future studies should address precisely how the PARP-dependent and PARP-independent functions of SMARCA5 contribute to the signaling and repair of DSBs. Taken together, our findings reveal that the interplay between DNA damage-induced PARylation, SMARCA5-mediated chromatin remodeling and the RNF8/RNF168 ubiquitin cascade regulates the cellular response to DSBs and as such promotes genomic stability in response to genetic insult.

Materials and Methods

Cell culture and chemicals

U2OS, HEK293, HeLa, VH10-SV40, VH10-hTERT and XP2OS-SV immortalized fibroblasts were grown in DMEM (Gibco) containing 10% FCS (Bodinco BV). GFP-XPA was expressed in XP2OS-SV cells, which are deficient in XPA (Rademakers et al., 2003). U2OS cells stably expressing GFP-MDC1, FLAG-RNF8, GFP-RNF168 or GFP-53BP1 were gifts from Jiri Lukas. pGFP-RNF8, pGFP-RAP80, pGFP-RAD18, pGFP-PARP1, pmCherry-PARG-WT, pmCherry-PARG-mut, pSMARCA5-WT-GFP and pSMARCA5-K211R-GFP expression vectors were obtained from Jiri Lukas, Anton Jetten, Satoshi Tateishi, Valerie Schreiber, Michael Hendzel and Akira Yasui. pGFP-UBC13 was previously described (Marteijn et al., 2009). pmCherry-RNF8 and pmCherry-RNF168 were made by replacing GFP with mCherry in pGFP-RNF8. pPAGFP-H2A was generated by replacing GFP with PAGFP in the previously described vector pGFP-H2A (Luijsterburg et al., 2012b). The cDNA for human SMARCA5 (Open Biosystems) was cloned into pEGFP-N1 (Clontech). SMARCA5-GFP was stably expressed in U2OS cells. siRNA and plasmid transfections were performed using HiPerfect (Qiagen), Lipofectamine RNAiMAX (Invitrogen), Lipofectamine 2000 (Invitrogen) and JetPEI (Polyplus Transfection), respectively, according to the manufacturer's instructions. The following siRNA sequences were used: 5′-CGUACGCGGAAUACUUCGA-3′ (Luciferase), 5′-GGAUUAAACUGGCUCA-UUU-3′ (SMARCA5-1, Dharmacon), 5′-GAGGAGAUGUAAUACCUUAUU-3′ (SMARCA5-2, Dharmacon), 5′-GGAAUGGUAUACUCGGAUA-3′ (SMARC-A5-5, Dharmacon), 5′-GGGCAAAUAGAUUCGAGUA-3′ (SMARCA5-6, Dharmacon), 5′-GAGGGCCAAUGGACAAUUA-3′ (RNF8, Dharmacon), 5′-GAAAGUGUUCAACUAAU-3′ (PARP1, Dharmacon), 5′-AAGGAUUGCUU-CAAGGUAA-3′ (PARP2, Dharmacon), 5′-AUAUGUUGGUGAACUGAGA-3′ (XRCC4) (Sartori et al., 2007), 5′-GAAGAAUGCAGGUUUAAUA-3′ (BRCA2, MWG). siRNAs against RNF168 were used as described (Doil et al., 2009). Cells were examined 48 h after siRNA transfection unless otherwise stated. ATM inhibitor (KU-55933) and PARPi (KU-0058948) were gifts from Mark O'Connor and used at a concentration of 10 μM unless stated otherwise. DNA-PK inhibitor (NU7026, EMD Biosciences) and ADP-HPD ammonium salt dehydrate (Santa Cruz) were used at a concentration of 10 μM, whereas *N*-methyl-*N*′-nitro-*N*-nitrosoguanidine (MNNG; Sigma) was used at a concentration of 100 μM.

Generation of DSBs

IR was delivered by a YXlon X-ray generator (YXlon International, 200 KV, 4 mA, dose rate 1.1 Gy/min).

Cell survival assay

VH10-SV40 cells were transfected for 48 h, trypsinized, seeded at low density and exposed to IR or PARPi. 7 days later cells were washed with 0.9% NaCl and stained with Methylene Blue. Colonies of more than 20 cells were scored.

Microscopy and laser micro-irradiation

Brightfield pictures were taken with an EVOS fl fluorescence microscope (AMG, Westover Scientific) using the 4× Ph objective. Laser micro-irradiation was carried out on a Leica SP5 confocal microscope equipped with an environmental chamber set to 37℃ and 5% CO_2. DSB-containing tracks (1.5 μm width) were generated with a Mira modelocked Ti:Sapphire laser (λ=800 nm, pulse length=200 fs, repetition rate=76 MHz, output power=80 mW). Confocal images were recorded before and after laser irradiation at different time intervals and analyzed using LAS-AF software. Fluorescence intensities were subtracted by the pre-bleach values and normalized to the first datapoint, which was set to 0, to obtain relative fluorescence units (RFU). Track width was measured using ImageJ software. PA–GFP-H2A was photoactivated using the same laser and settings as those used to inflict localized DNA damage.

ATP depletion

Cells were rinsed with PBS and incubated in ATP depletion medium (137 mM NaCl, 5.4 mM KCl, 1.8 mM $CaCl_2$, 0.8 mM $MgSO_4$, 60 mM deoxyglucose, 30 mM NaAz, 20 mM HEPES and 10% FCS) or mock medium (137 mM NaCl, 5.4 mM KCl, 1.8 mM $CaCl_2$, 0.8 mM $MgSO_4$, 20 mM D-glucose, 20 mM HEPES and 10% FCS) at 37℃ as described previously (Luijsterburg et al., 2012b). Cells were then transferred to the microscope chamber and subjected to multiphoton micro-irradiation.

Antibodies

Immunofluorescence and western blot analysis were performed using antibodies to γH2AX, phospho-histone H3 S10p (Millipore), α-Tubulin (Sigma), Streptavidin (IBA BioTAGnology), GFP (Roche), ubiquitin and PARP2 (FK2, Enzo Life Sciences), PAR (Trevigen), BRCA1 (Calbiochem and Santa Cruz), 53BP1 (Novus), SMARCA5/SNF2h, histone H3 and MDC1 (Abcam) and PARP1 (Cell Signaling). The antibodies to RNF168, 53BP1, RAD51 and XRCC4 were gifts from Daniel Durocher, Thanos Halozanetis, Roland Kanaar and Mauro Modesti, respectively.

IRIF analysis

IRIF were analyzed using home-made Stacks software as described previously (Smeenk et al., 2010). Statistical significance was established at each timepoint using one-way ANOVA.

Complementation assay

Cells were transfected twice using siRNA against SMARCA5 (SMARCA5-1). Two days after the first transfection cells were transfected with pGFP, pSMARCA5-WT-GFP or pSMARCA5-K211R-GFP plasmid DNA and 1 day later irradiated and analyzed by immunoblotting and fluorescence microscopy.

Ubiquitylation assay

Chromatin-enriched extracts were prepared and used for immunoprecipitation of γH2AX as described previously (Smeenk et al., 2010).

Protein interaction studies

To study the RNF168-SMARCA5 interaction cells were lysed in EBC buffer (50 mM Tris, pH 7.5, 150 mM NaCl, 0.5% NP-40, 1 mM EDTA) supplemented with protease and phosphatase inhibitor cocktails. Cleared lysates were subjected to immunoprecipitation with GFP Trap beads (Chromotek), Strep-Tactin Sepharose (IBA BioTAGnology) or RNF168 antibody for 1.5 h. Beads were washed four times with EBC buffer and boiled in sample buffer. Bound proteins were resolved by SDS-PAGE and processed for immunoblotting. For mass spectrometric analysis of the RNF168-SMARCA5 interaction, RNF168 immunoprecipitates from cells subjected to stable isotope labeling by amino acids in cell culture (SILAC; 7 days) were eluted from beads with 0.1 M glycine (pH 2.5) and analyzed on an LTQ-Orbitrap Velos mass spectrometer (Thermo Fisher Scientific) (Ong et al., 2003). Data analysis was performed with MaxQuant software.

PARylation assay

Cells were transfected with pGFP, pGFP-PARP1, pSMARCA5-GFP and pGFP-RNF168 and after 2 days either irradiated or treated with MNNG for 5 minutes. Cells were collected in PBS and then lysed in RIPA buffer (10 mM Tris, pH 8.0, 450 mM NaCl, 1% Triton X-100, 0.1% deoxycholate, 0.1% SDS) supplemented with protease inhibitor cocktails. Cleared lysates were subjected to immunoprecipitation with GFP Trap beads (Chromotek) for 2 h. The beads were then washed with RIPA buffer (three times), RIPA buffer supplemented with 1 M NaCl (2 times) and TBS supplemented with 0.1% Tween. All buffers contained PARG inhibitor. Bound proteins were resolved by SDS-PAGE and processed for immunoblotting. The Odyssey imager (Li-Cor Biosciences) equipped with Li-Cor Odyssey 3.0 software was used to scan the membranes and analyze the fluorescence signals.

Homologous recombination and non-homologous end-joining assays

HEK293 cell lines containing either a stably integrated copy of the DR-GFP or EJ5-GFP reporter were used to measure the repair of I-S*ce*I-induced DSBs by HR or NHEJ, respectively (Bennardo et al., 2008; Pierce et al., 1999). Briefly, 48 h after siRNA transfection, cells were transfected with the I-S*ce*I expression vector pCBASce and a RFP expression vector (Pierce et al., 1999). 48 h later the fraction of GFP-positive cells among the RFP-positive cells was determined by FACS on a BD LSRII flow cytometer (BD Bioscience) using FACSDiva software version 5.0.3. Quantifications were performed using WinMDI 2.9 software.

Acknowledgements

We thank Mark O'Connor, Jiri Lukas, Dan Durocher, Maria Jasin, Jeremy Stark, Mauro Modesti, Roland Kanaar, Thanos Halozanetis, Gaëlle Legube, Anton Jetten, Satoshi Tateishi, Valerie Schreiber,

Michael Hendzel and Akira Yasui for reagents, and acknowledge Robin van Schendel for assistance with the HR assay and Annelies van der Laan and Hans Tanke for facilitating laser micro-irradiation experiments.

Author contributions

G.S., J.A.M., M.S.L., N.M., A.P. and H.V.A. conceived and designed experiments. G.S., W.W.W., J.A.M., M.S.L., N.S., T.C. and R.J.R. performed experiments. G.S., W.W.W., J.A.M., M.S.L., T.C., N.M., W.V. and H.V.A. analysed the data. G.S., M.S.L. and H.V.A. wrote the manuscript.

Funding

This work was funded by a Vidi grant from The Netherlands Organization for Scientific Research [grant number 864.07.001 to H.V.A.]; a CDA grant from The Human Frontier Science Program [grant number CDA00048/2009 to H.V.A.]; and Veni grants from The Netherlands Organization for Scientific Research [grant numbers 916.96.120, 863.11.007 to J.A.M. and M.S.L.].

Supplementary material available online at
http://jcs.biologists.org/lookup/suppl/doi:10.1242/jcs.109413/-/DC1

References

Ahel, D., Horejsí, Z., Wiechens, N., Polo, S. E., Garcia-Wilson, E., Ahel, I., Flynn, H., Skehel, M., West, S. C., Jackson, S. P. et al. (2009). Poly(ADP-ribose)-dependent regulation of DNA repair by the chromatin remodeling enzyme ALC1. *Science* **325**, 1240-1243.

Bao, Y. and Shen, X. (2007). SnapShot: Chromatin Remodeling Complexes. *Cell* **129**, 632.e1–632.e2.

Barak, O., Lazzaro, M. A., Lane, W. S., Speicher, D. W., Picketts, D. J. and Shiekhattar, R. (2003). Isolation of human NURF: a regulator of Engrailed gene expression. *EMBO J.* **22**, 6089-6100.

Bekker-Jensen, S. and Mailand, N. (2010). Assembly and function of DNA double-strand break repair foci in mammalian cells. *DNA Repair (Amst.)* **9**, 1219-1228.

Bekker-Jensen, S., Rendtlew Danielsen, J., Fugger, K., Gromova, I., Nerstedt, A., Lukas, C., Bartek, J., Lukas, J. and Mailand, N. (2010). HERC2 coordinates ubiquitin-dependent assembly of DNA repair factors on damaged chromosomes. *Nat. Cell Biol.* **12**, 80-86.

Bennardo, N., Cheng, A., Huang, N. and Stark, J. M. (2008). Alternative-NHEJ is a mechanistically distinct pathway of mammalian chromosome break repair. *PLoS Genet.* **4**, e1000110.

Boehler, C., Gauthier, L. R., Mortusewicz, O., Biard, D. S., Saliou, J. M., Bresson, A., Sanglier-Cianferani, S., Smith, S., Schreiber, V., Boussin, F. et al. (2011). Poly(ADP-ribose) polymerase 3 (PARP3), a newcomer in cellular response to DNA damage and mitotic progression. *Proc. Natl. Acad. Sci. USA* **108**, 2783-2788.

Chou, D. M., Adamson, B., Dephoure, N. E., Tan, X., Nottke, A. C., Hurov, K. E., Gygi, S. P., Colaiácovo, M. P. and Elledge, S. J. (2010). A chromatin localization screen reveals poly (ADP ribose)-regulated recruitment of the repressive polycomb and NuRD complexes to sites of DNA damage. *Proc. Natl. Acad. Sci. USA* **107**, 18475-18480.

Collins, N., Poot, R. A., Kukimoto, I., García-Jiménez, C., Dellaire, G. and Varga-Weisz, P. D. (2002). An ACF1-ISWI chromatin-remodeling complex is required for DNA replication through heterochromatin. *Nat. Genet.* **32**, 627-632.

Doil, C., Mailand, N., Bekker-Jensen, S., Menard, P., Larsen, D. H., Pepperkok, R., Ellenberg, J., Panier, S., Durocher, D., Bartek, J. et al. (2009). RNF168 binds and amplifies ubiquitin conjugates on damaged chromosomes to allow accumulation of repair proteins. *Cell* **136**, 435-446.

Doyon, Y. and Côté, J. (2004). The highly conserved and multifunctional NuA4 HAT complex. *Curr. Opin. Genet. Dev.* **14**, 147-154.

Erdel, F., Schubert, T., Marth, C., Längst, G. and Rippe, K. (2010). Human ISWI chromatin-remodeling complexes sample nucleosomes via transient binding reactions and become immobilized at active sites. *Proc. Natl. Acad. Sci. USA* **107**, 19873-19878.

Gagné, J.-P., Isabelle, M., Lo, K. S., Bourassa, S., Hendzel, M. J., Dawson, V. L., Dawson, T. M. and Poirier, G. G. (2008). Proteome-wide identification of poly(ADP-ribose) binding proteins and poly(ADP-ribose)-associated protein complexes. *Nucleic Acids Res.* **36**, 6959-6976.

Gottschalk, A. J., Timinszky, G., Kong, S. E., Jin, J., Cai, Y., Swanson, S. K., Washburn, M. P., Florens, L., Ladurner, A. G., Conaway, J. W. et al. (2009). Poly(ADP-ribosyl)ation directs recruitment and activation of an ATP-dependent chromatin remodeler. *Proc. Natl. Acad. Sci. USA* **106**, 13770-13774.

Gudjonsson, T., Altmeyer, M., Savic, V., Toledo, L., Dinant, C., Grøfte, M., Bartkova, J., Poulsen, M., Oka, Y., Bekker-Jensen, S. et al. (2012). TRIP12 and UBR5 suppress spreading of chromatin ubiquitylation at damaged chromosomes. *Cell* **150**, 697-709.

Haince, J. F., McDonald, D., Rodrigue, A., Déry, U., Masson, J. Y., Hendzel, M. J. and Poirier, G. G. (2008). PARP1-dependent kinetics of recruitment of MRE11 and NBS1 proteins to multiple DNA damage sites. *J. Biol. Chem.* **283**, 1197-1208.

Huang, J., Huen, M. S., Kim, H., Leung, C. C., Glover, J. N., Yu, X. and Chen, J. (2009). RAD18 transmits DNA damage signalling to elicit homologous recombination repair. *Nat. Cell Biol.* **11**, 592-603.

Huen, M. S. and Chen, J. (2010). Assembly of checkpoint and repair machineries at DNA damage sites. *Trends Biochem. Sci.* **35**, 101-108.

Huen, M. S., Grant, R., Manke, I., Minn, K., Yu, X., Yaffe, M. B. and Chen, J. (2007). RNF8 transduces the DNA-damage signal via histone ubiquitylation and checkpoint protein assembly. *Cell* **131**, 901-914.

Iacovoni, J. S., Caron, P., Lassadi, I., Nicolas, E., Massip, L., Trouche, D. and Legube, G. (2010). High-resolution profiling of gammaH2AX around DNA double strand breaks in the mammalian genome. *EMBO J.* **29**, 1446-1457.

Ismail, I. H., Gagné, J. P., Caron, M. C., McDonald, D., Xu, Z., Masson, J. Y., Poirier, G. G. and Hendzel, M. J. (2012). CBX4-mediated SUMO modification regulates BMI1 recruitment at sites of DNA damage. *Nucleic Acids Res.* **40**, 5497-5510.

Ito, T., Levenstein, M. E., Fyodorov, D. V., Kutach, A. K., Kobayashi, R. and Kadonaga, J. T. (1999). ACF consists of two subunits, Acf1 and ISWI, that function cooperatively in the ATP-dependent catalysis of chromatin assembly. *Genes Dev.* **13**, 1529-1539.

Jackson, S. P. and Bartek, J. (2009). The DNA-damage response in human biology and disease. *Nature* **461**, 1071-1078.

Kim, M. Y., Zhang, T. and Kraus, W. L. (2005). Poly(ADP-ribosyl)ation by PARP-1: 'PAR-laying' NAD+ into a nuclear signal. *Genes Dev.* **19**, 1951-1967.

Kim, H., Chen, J. and Yu, X. (2007). Ubiquitin-binding protein RAP80 mediates BRCA1-dependent DNA damage response. *Science* **316**, 1202-1205.

Kolas, N. K., Chapman, J. R., Nakada, S., Ylanko, J., Chahwan, R., Sweeney, F. D., Panier, S., Mendez, M., Wildenhain, J., Thomson, T. M. et al. (2007). Orchestration of the DNA-damage response by the RNF8 ubiquitin ligase. *Science* **318**, 1637-1640.

Kruhlak, M. J., Celeste, A., Dellaire, G., Fernandez-Capetillo, O., Müller, W. G., McNally, J. G., Bazett-Jones, D. P. and Nussenzweig, A. (2006). Changes in chromatin structure and mobility in living cells at sites of DNA double-strand breaks. *J. Cell Biol.* **172**, 823-834.

Lan, L., Ui, A., Nakajima, S., Hatakeyama, K., Hoshi, M., Watanabe, R., Janicki, S. M., Ogiwara, H., Kohno, T., Kanno, S.-I. et al. (2010). The ACF1 complex is required for DNA double-strand break repair in human cells. *Mol. Cell* **40**, 976-987.

Larsen, D. H., Poinsignon, C., Gudjonsson, T., Dinant, C., Payne, M. R., Hari, F. J., Rendtlew Danielsen, J. M., Menard, P., Sand, J. C., Stucki, M. et al. (2010). The chromatin-remodeling factor CHD4 coordinates signaling and repair after DNA damage. *J. Cell Biol.* **190**, 731-740.

Lee, J. H., Goodarzi, A. A., Jeggo, P. A. and Paull, T. T. (2010). 53BP1 promotes ATM activity through direct interactions with the MRN complex. *EMBO J.* **29**, 574-585.

LeRoy, G., Loyola, A., Lane, W. S. and Reinberg, D. (2000). Purification and characterization of a human factor that assembles and remodels chromatin. *J. Biol. Chem.* **275**, 14787-14790.

Luijsterburg, M. S. and van Attikum, H. (2011). Chromatin and the DNA damage response: the cancer connection. *Mol. Oncol.* **5**, 349-367.

Luijsterburg, M. S. and van Attikum, H. (2012). Close encounters of the RNF8th kind: when chromatin meets DNA repair. *Curr. Opin. Cell Biol.* **24**, 439-447.

Luijsterburg, M. S., Acs, K., Ackermann, L., Wiegant, W. W., Bekker-Jensen, S., Larsen, D. H., Khanna, K. K., van Attikum, H., Mailand, N. and Dantuma, N. P. (2012a). A new non-catalytic role for ubiquitin ligase RNF8 in unfolding higher-order chromatin structure. *EMBO J.* **31**, 2511-2527.

Luijsterburg, M. S., Lindh, M., Acs, K., Vrouwe, M. G., Pines, A., van Attikum, H., Mullenders, L. H. and Dantuma, N. P. (2012b). DDB2 promotes chromatin decondensation at UV-induced DNA damage. *J. Cell Biol.* **197**, 267-281.

Mailand, N., Bekker-Jensen, S., Faustrup, H., Melander, F., Bartek, J., Lukas, C. and Lukas, J. (2007). RNF8 ubiquitylates histones at DNA double-strand breaks and promotes assembly of repair proteins. *Cell* **131**, 887-900.

Marteijn, J. A., Bekker-Jensen, S., Mailand, N., Lans, H., Schwertman, P., Gourdin, A. M., Dantuma, N. P., Lukas, J. and Vermeulen, W. (2009). Nucleotide excision repair-induced H2A ubiquitination is dependent on MDC1 and RNF8 and reveals a universal DNA damage response. *J. Cell Biol.* **186**, 835-847.

McCabe, N., Turner, N. C., Lord, C. J., Kluzek, K., Bialkowska, A., Swift, S., Giavara, S., O'Connor, M. J., Tutt, A. N., Zdzienicka, M. Z. et al. (2006). Deficiency in the repair of DNA damage by homologous recombination and sensitivity to poly(ADP-ribose) polymerase inhibition. *Cancer Res.* **66**, 8109-8115.

Messner, S. and Hottiger, M. O. (2011). Histone ADP-ribosylation in DNA repair, replication and transcription. *Trends Cell Biol.* **21**, 534-542.

Moynahan, M. E., Pierce, A. J. and Jasin, M. (2001). BRCA2 is required for homology-directed repair of chromosomal breaks. *Mol. Cell* **7**, 263-272.

Murr, R., Loizou, J. I., Yang, Y. G., Cuenin, C., Li, H., Wang, Z. Q. and Herceg, Z. (2006). Histone acetylation by Trrap-Tip60 modulates loading of repair proteins and repair of DNA double-strand breaks. *Nat. Cell Biol.* **8**, 91-99.

Nakada, S., Tai, I., Panier, S., Al-Hakim, A., Iemura, S., Juang, Y. C., O'Donnell, L., Kumakubo, A., Munro, M., Sicheri, F. et al. (2010). Non-canonical inhibition of DNA damage-dependent ubiquitination by OTUB1. *Nature* **466**, 941-946.

Nakamura, K., Kato, A., Kobayashi, J., Yanagihara, H., Sakamoto, S., Oliveira, D. V. N. P., Shimada, M., Tauchi, H., Suzuki, H., Tashiro, S. et al. (2011).

Regulation of homologous recombination by RNF20-dependent H2B ubiquitination. *Mol. Cell* **41**, 515-528.

Negrini, S., Gorgoulis, V. G. and Halazonetis, T. D. (2010). Genomic instability – an evolving hallmark of cancer. *Nat. Rev. Mol. Cell Biol.* **11**, 220-228.

Ong, S. E., Foster, L. J. and Mann, M. (2003). Mass spectrometric-based approaches in quantitative proteomics. *Methods* **29**, 124-130.

Park, J. H., Park, E. J., Lee, H. S., Kim, S. J., Hur, S. K., Imbalzano, A. N. and Kwon, J. (2006). Mammalian SWI/SNF complexes facilitate DNA double-strand break repair by promoting gamma-H2AX induction. *EMBO J.* **25**, 3986-3997.

Patterson, G. H. and Lippincott-Schwartz, J. (2002). A photoactivatable GFP for selective photolabeling of proteins and cells. *Science* **297**, 1873-1877.

Pierce, A. J., Johnson, R. D., Thompson, L. H. and Jasin, M. (1999). XRCC3 promotes homology-directed repair of DNA damage in mammalian cells. *Genes Dev.* **13**, 2633-2638.

Poirier, G. G., de Murcia, G., Jongstra-Bilen, J., Niedergang, C. and Mandel, P. (1982). Poly(ADP-ribosyl)ation of polynucleosomes causes relaxation of chromatin structure. *Proc. Natl. Acad. Sci. USA* **79**, 3423-3427.

Polo, S. E., Kaidi, A., Baskcomb, L., Galanty, Y. and Jackson, S. P. (2010). Regulation of DNA-damage responses and cell-cycle progression by the chromatin remodelling factor CHD4. *EMBO J.* **29**, 3130-3139.

Poot, R. A., Dellaire, G., Hülsmann, B. B., Grimaldi, M. A., Corona, D. F., Becker, P. B., Bickmore, W. A. and Varga-Weisz, P. D. (2000). HuCHRAC, a human ISWI chromatin remodelling complex contains hACF1 and two novel histone-fold proteins. *EMBO J.* **19**, 3377-3387.

Rademakers, S., Volker, M., Hoogstraten, D., Nigg, A. L., Moné, M. J., Van Zeeland, A. A., Hoeijmakers, J. H., Houtsmuller, A. B. and Vermeulen, W. (2003). Xeroderma pigmentosum group A protein loads as a separate factor onto DNA lesions. *Mol. Cell Biol.* **23**, 5755-5767.

Sánchez-Molina, S., Mortusewicz, O., Bieber, B., Auer, S., Eckey, M., Leonhardt, H., Friedl, A. A. and Becker, P. B. (2011). Role for hACF1 in the G2/M damage checkpoint. *Nucleic Acids Res.* **39**, 8445-8456.

Sartori, A. A., Lukas, C., Coates, J., Mistrik, M., Fu, S., Bartek, J., Baer, R., Lukas, J. and Jackson, S. P. (2007). Human CtIP promotes DNA end resection. *Nature* **450**, 509-514.

Smeenk, G., Wiegant, W. W., Vrolijk, H., Solari, A. P., Pastink, A. and van Attikum, H. (2010). The NuRD chromatin-remodeling complex regulates signaling and repair of DNA damage. *J. Cell Biol.* **190**, 741-749.

Sobhian, B., Shao, G., Lilli, D. R., Culhane, A. C., Moreau, L. A., Xia, B., Livingston, D. M. and Greenberg, R. A. (2007). RAP80 targets BRCA1 to specific ubiquitin structures at DNA damage sites. *Science* **316**, 1198-1202.

Stewart, G. S., Panier, S., Townsend, K., Al-Hakim, A. K., Kolas, N. K., Miller, E. S., Nakada, S., Ylanko, J., Olivarius, S., Mendez, M. et al. (2009). The RIDDLE syndrome protein mediates a ubiquitin-dependent signaling cascade at sites of DNA damage. *Cell* **136**, 420-434.

Stucki, M., Clapperton, J. A., Mohammad, D., Yaffe, M. B., Smerdon, S. J. and Jackson, S. P. (2005). MDC1 directly binds phosphorylated histone H2AX to regulate cellular responses to DNA double-strand breaks. *Cell* **123**, 1213-1226.

van Attikum, H. and Gasser, S. M. (2009). Crosstalk between histone modifications during the DNA damage response. *Trends Cell Biol.* **19**, 207-217.

van Haaften, G., Romeijn, R., Pothof, J., Koole, W., Mullenders, L. H., Pastink, A., Plasterk, R. H. and Tijsterman, M. (2006). Identification of conserved pathways of DNA-damage response and radiation protection by genome-wide RNAi. *Curr. Biol.* **16**, 1344-1350.

Wang, B., Matsuoka, S., Ballif, B. A., Zhang, D., Smogorzewska, A., Gygi, S. P. and Elledge, S. J. (2007). Abraxas and RAP80 form a BRCA1 protein complex required for the DNA damage response. *Science* **316**, 1194-1198.

Weinstock, D. M., Nakanishi, K., Helgadottir, H. R. and Jasin, M. (2006). Assaying double-strand break repair pathway choice in mammalian cells using a targeted endonuclease or the RAG recombinase. *Methods Enzymol.* **409**, 524-540.

Wu, J., Huen, M. S., Lu, L. Y., Ye, L., Dou, Y., Ljungman, M., Chen, J. and Yu, X. (2009). Histone ubiquitination associates with BRCA1-dependent DNA damage response. *Mol. Cell. Biol.* **29**, 849-860.

Wyman, C. and Kanaar, R. (2006). DNA double-strand break repair: all's well that ends well. *Annu. Rev. Genet.* **40**, 363-383.

Xu, Y., Sun, Y., Jiang, X., Ayrapetov, M. K., Moskwa, P., Yang, S., Weinstock, D. M. and Price, B. D. (2010). The p400 ATPase regulates nucleosome stability and chromatin ubiquitination during DNA repair. *J. Cell Biol.* **191**, 31-43.

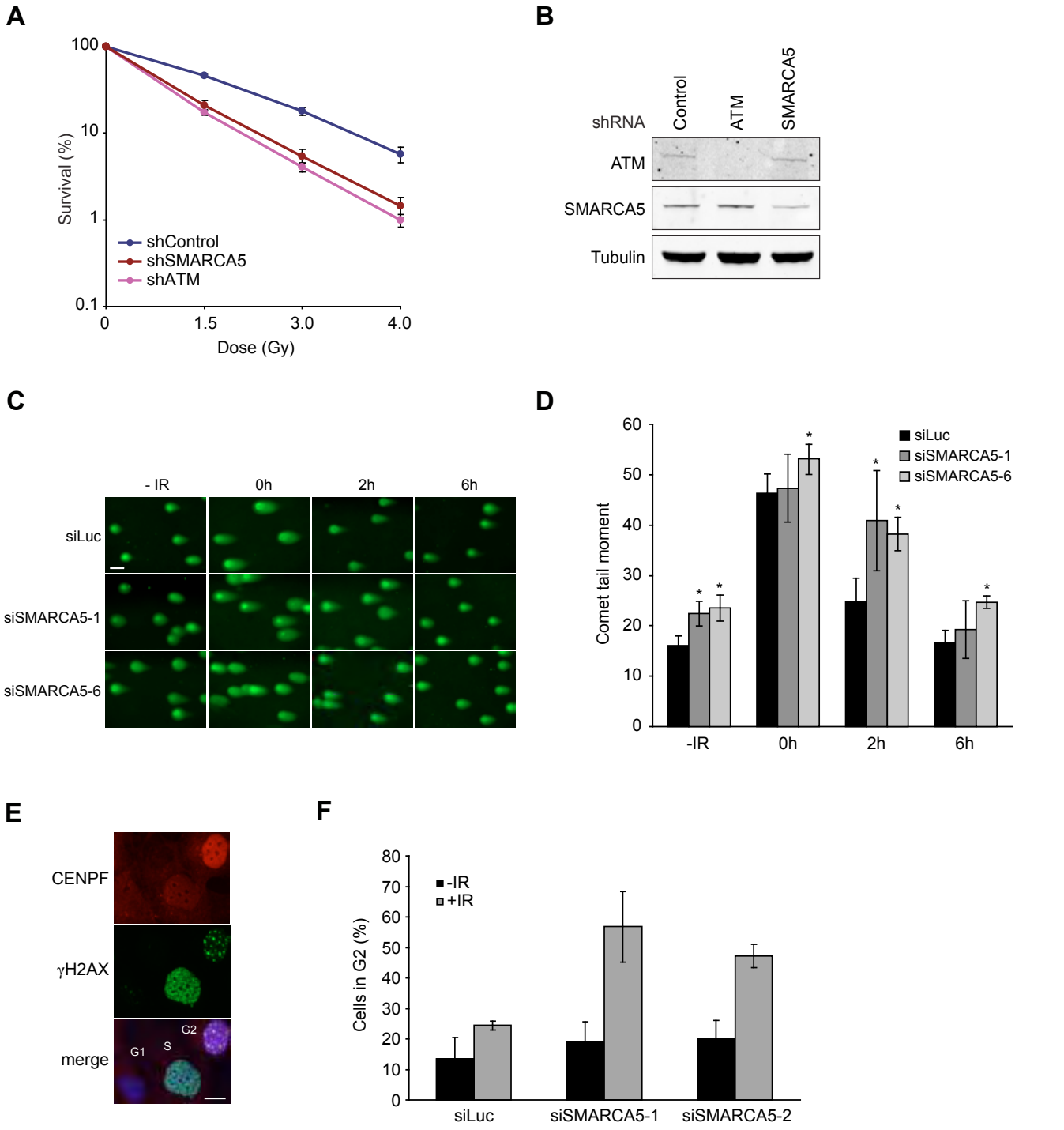

Fig. S1. SMARCA5 depletion renders cells hypersensitive to IR and impairs DSB repair and cell cycle progression after IR. (**A**) VH10-hTERT cells stably expressing an shRNA against SMARCA5 (5′-GATCCCCGTGTTTGCTTCAAAGGAAATTCAAGAGATTTCCTTTGAAGCAAACACTTTTT-3′) or ATM displayed increased IR sensitivity when compared to control cells stably expressing mouse HIF1 shRNA in clonogenic survival assays (van Haaften et al., 2006). Graphs represent the mean ± s.e.m. of 3 independent experiments. (**B**) SMARCA5 and ATM levels were monitored by western blot analysis using WCE of cells in A. Tubulin is a loading control. (**C**) VH10-hTERT cells were transfected with the indicated siRNAs for 72 h, exposed to 20 Gy IR and subjected to neutral comet analysis at the indicated time points using the Comet Assay system (Trevigen) according to the manufacturer's instructions. Representative images are shown. Scale bar, 30 μm. (**D**) Quantification of tail moments using cells from C. Comet tail moments were scored using Comet Score software (TriTek). Tail moments for each condition were calculated for at least 100 cells per data point. The mean ± s.e.m. of 3 experiments is shown. Statistical significance was established at each timepoint using a student t-test. **P*<0.05, compared with siLuc (control). (**E**) Knockdown of SMARCA5 induces a G2 cell cycle arrest after exposure of cells to IR. U2OS cells were exposed to 5 Gy IR or left untreated and after 18 h immunostained for γH2AX and CENP-F (using anti-CENP-F antibody; Santa Cruz). DNA was stained with DAPI. The levels of CENP-F staining distinguished G1, S and G2 cells. Scale bar, 10 μm. (**F**) The percentage of G2 cells ± s.e.m. is presented. More than 120 nuclei were scored per sample in at least 2 independent experiments.

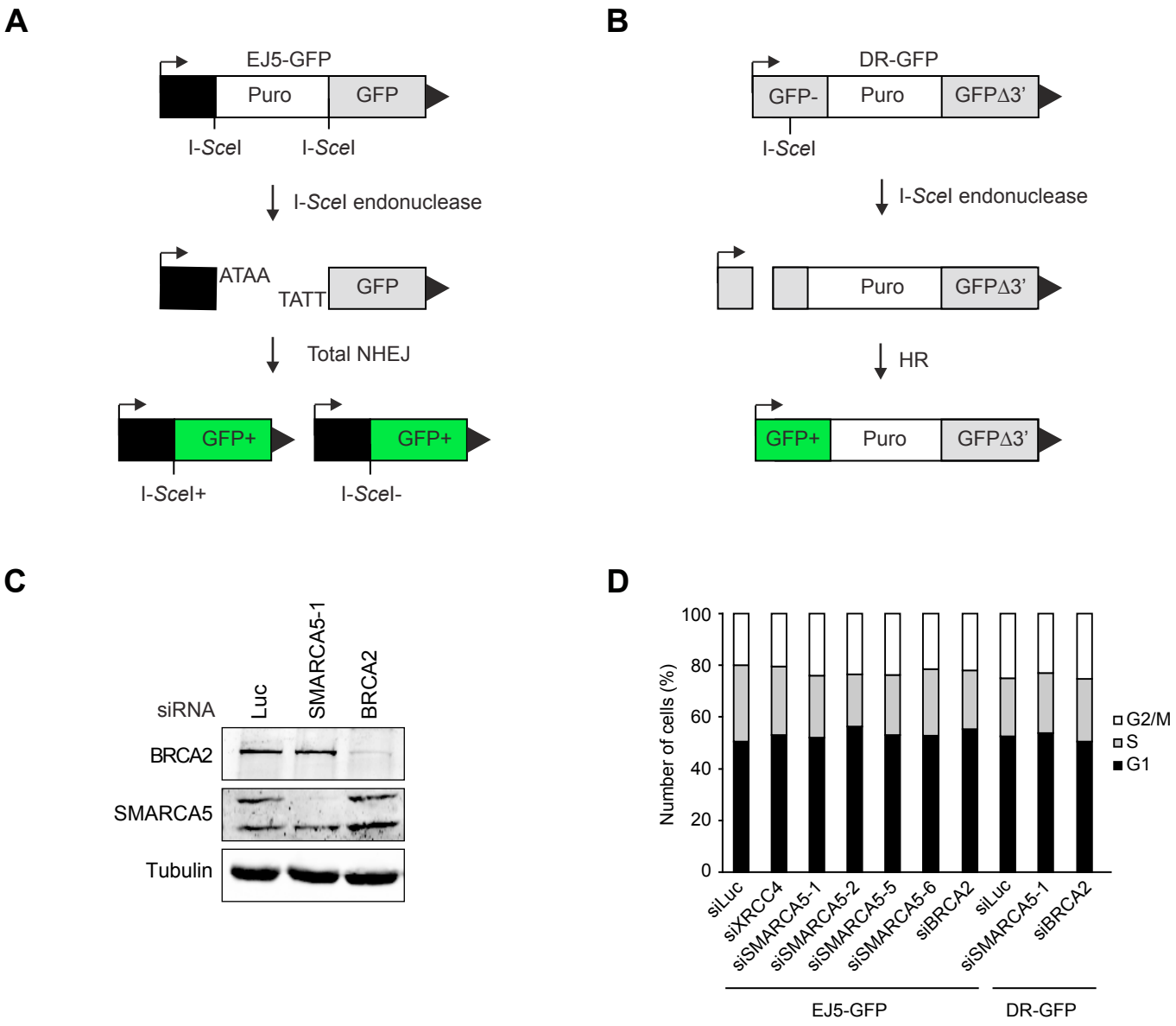

Fig. S2. SMARCA5 depletion does not affect cell cycle progression in NHEJ and HR reporter cell systems. (**A**) Schematic representation of a reporter system for NHEJ. EJ5-GFP consists of a promoter that is separated from a GFP cassette by insertion of a puromycin resistance marker flanked by I-S*ce*I recognition sites (Bennardo et al., 2008). After transient expression of I-S*ce*I and subsequent cleavage at these sites, NHEJ (either error-free or error-prone) will fuse the promoter to GFP and restore expression. (**B**) Schematic representation of a reporter system for HR. DR-GFP consists of two GFP alleles that are non-functional due to the insertion of an I-S*ce*I recognition site and a 3′ truncation, respectively (Weinstock et al., 2006). After transient expression of I-S*ce*I and subsequent cleavage at the I-S*ce*I recognition site, HR will use the GFPΔ3′ as a template to repair the DSB, which will restore GFP expression. (**C**) SMARCA5 and BRCA2 levels were monitored by western blot analysis using WCE from cells in figure 1D. Tubulin is a loading control. (**D**) HEK293T cells containing the EJ5-GFP or DR-GFP reporter system were transfected with the indicated siRNAs. After 48 h cells were stained with propidium iodide and subjected to FACS. Percentage of cells in G1 (black bar), S (grey bar) and G2/M (white bar) phase is represented. Data shown are the average of 2 independent experiments.

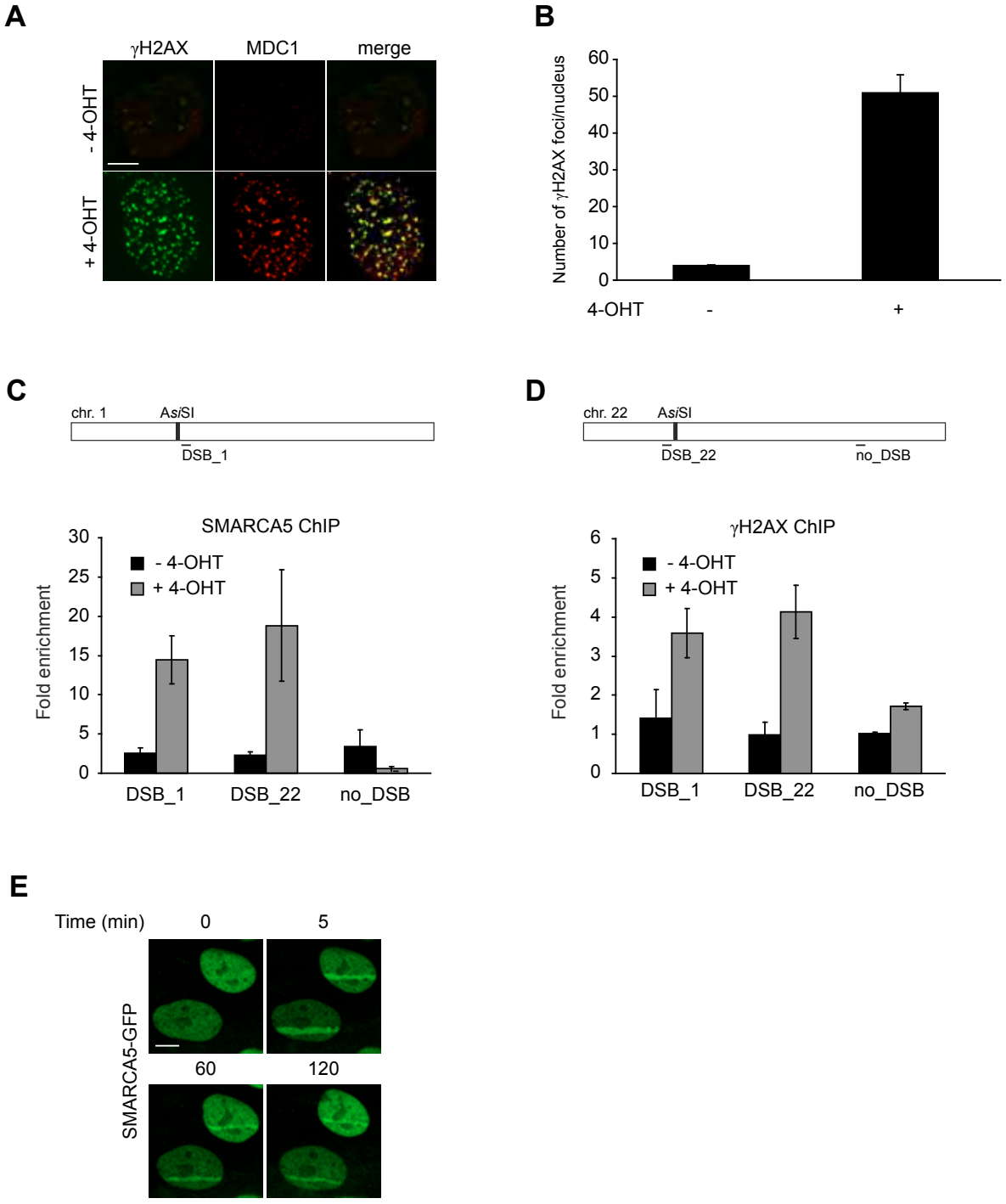

Fig. S3. SMARCA5 accumulates at site-specific DSBs and laser-induced DNA damage. (**A**) U2OS cells containing AsiSI-ER display increased 4-OHT-induced γH2AX and MDC1 foci. Cells containing A*si*SI-ER were untreated or treated with 300 nM 4-OHT for 4 h and subsequently immunostained for γH2AX and MDC1. (**B**) Quantitative analysis of γH2AX focus formation. The average number of foci/nucleus ± s.e.m. is presented. More than 150 nuclei from cells in A were scored per time point in at least 2 independent experiments. (**C**) Site-specific DSBs were induced by treatment of U2OS cells containing A*si*SI-ER with 300 nM 4-hydroxytamoxifen (4-OHT) for 4 hours. Cells were analyzed by ChIP using antibodies against SMARCA5, followed by qPCR using primers at the indicated distances from A*si*SI consensus sequences on chromosome 1 (position 89.231.183) and chromosome 22 (position 19.180.307) as described previously (Iacovoni et al., 2010). The following qPCR primers were used: DSB_1 forward 5′-GATTGGCTATGGGTGTGGAC-3′ and reverse 5′-CATCCTTGCAAACCAGTCCT-3′; DSB_22 forward 5′-CCTTCTTTCCCAGTGGTTCA-3′ and reverse 5′-GTGGTCTGACCCAGAGTGGT-3′; no_DSB forward 5′-CCCATCTCAACCTCCACACT-3′ and reverse 5′-CTTGTCCAGATTCGCTGTGA-3′; GAPDH forward 5′-GAAGGTGAAGGTCGGCGTCA-3′ and 5′-GAAGATGGTGATGGGATTTC-3′. Values for the cleaved (DSB_1 and DSB_22) and non-cleaved (no_DSB; 2 Mb distal to DSB_22) sites were normalized to those for the GAPDH control in ChIP and input samples. ChIP ratios were normalized to input ratios. (**D**) As in C, except that an antibody against γH2AX was used. (**E**) U2OS cells expressing SMARCA5-GFP were laser-irradiated and protein assembly at the damaged area was monitored at the indicated timepoints. Scale bars, 10 μm.

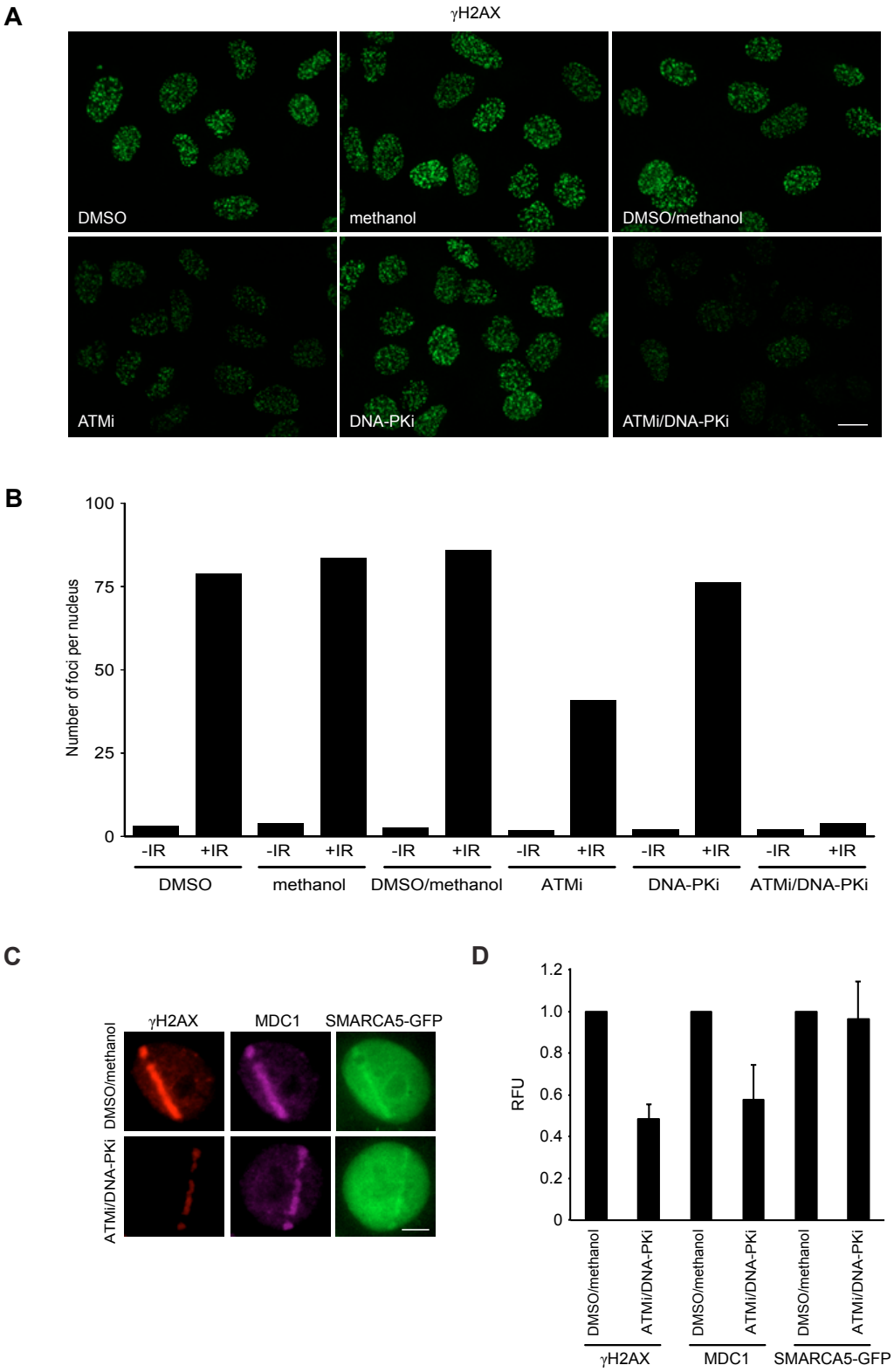

Fig. S4. Effect of ATM/DNA-PK inhibition on γH2AX, MDC1 and SMARCA5 accumulation at sites of DNA damage. (**A**) ATM and DNA-PK inhibition abrogates γH2AX IRIF formation. U2OS cells were treated with DMSO (control for ATM inhibitor), methanol (control for DNA-PK inhibitor) or inhibitors of ATM and DNA-PK, exposed to 2 Gy IR and 30 minutes later immunostained for γH2AX. (**B**) Quantitative representation of γH2AX IRIF formation in C. The average number of γH2AX foci/nucleus is presented. More than 150 nuclei were scored per sample. (**C**) ATM and DNA-PK inhibition reduces γH2AX and MDC1, but not SMARCA5 accumulation at sites of laser-induced DNA damage. U2OS cells expressing SMARCA5-GFP were treated with DMSO (control for ATM inhibitor) and methanol (control for DNA-PK inhibitor), or inhibitors of ATM and DNA-PK, then laser-irradiated and after 15 minutes immunostained for γH2AX and MDC1. (**D**) Quantitative representation of protein assembly at the damaged area in cells from A. Relative Fluorescence Units (RFU) are plotted on a time scale. Graphs represent the mean ± s.e.m. of at least 10 individual cells from 2 independent experiments. The RFU for control cells was set to 1. Scale bars, 10 μm.

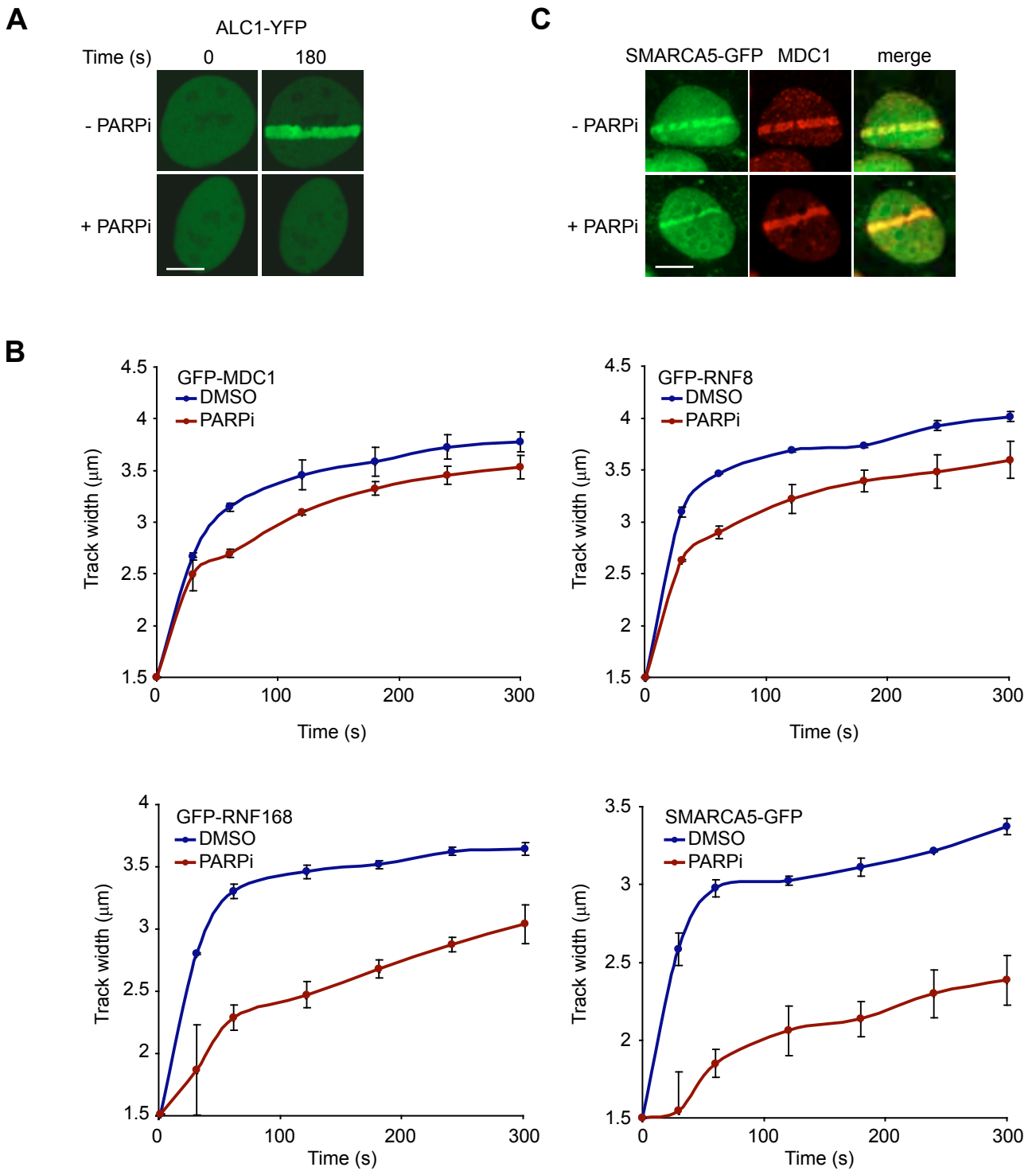

Fig. S5. PARP affects the occupancy of SMARCA5 and factors of the RNF168 cascade throughout damaged chromatin. (**A**) U2OS cells expressing ALC1-YFP were treated with PARP inhibitor or left untreated, and subjected to multi-photon laser-irradiation. Representative images illustrating the effect of PARP inhibition on the accumulation of ALC1-YFP at the indicated timepoints are shown Scale bars, 10 μm. (**B**) As in A, except that U2OS cells expressing GFP-MDC1, GFP-RNF8, GFP-RNF168 or SMARCA5-GFP were used. Moreover, tracks with a width of 1.5 μm were induced using a multiphoton laser and the subsequent increase in track width was measured up to 300 seconds after irradiation. The average track width +/- s.e.m. for at least 20 tracks from two independent experiments is presented. (**C**) As in A, except that U2OS cells expressing SMARCA5-GFP were used to examine the expansion of SMARCA5-GFP and immunostained endogenous MDC1 at 180 seconds after irradiation.

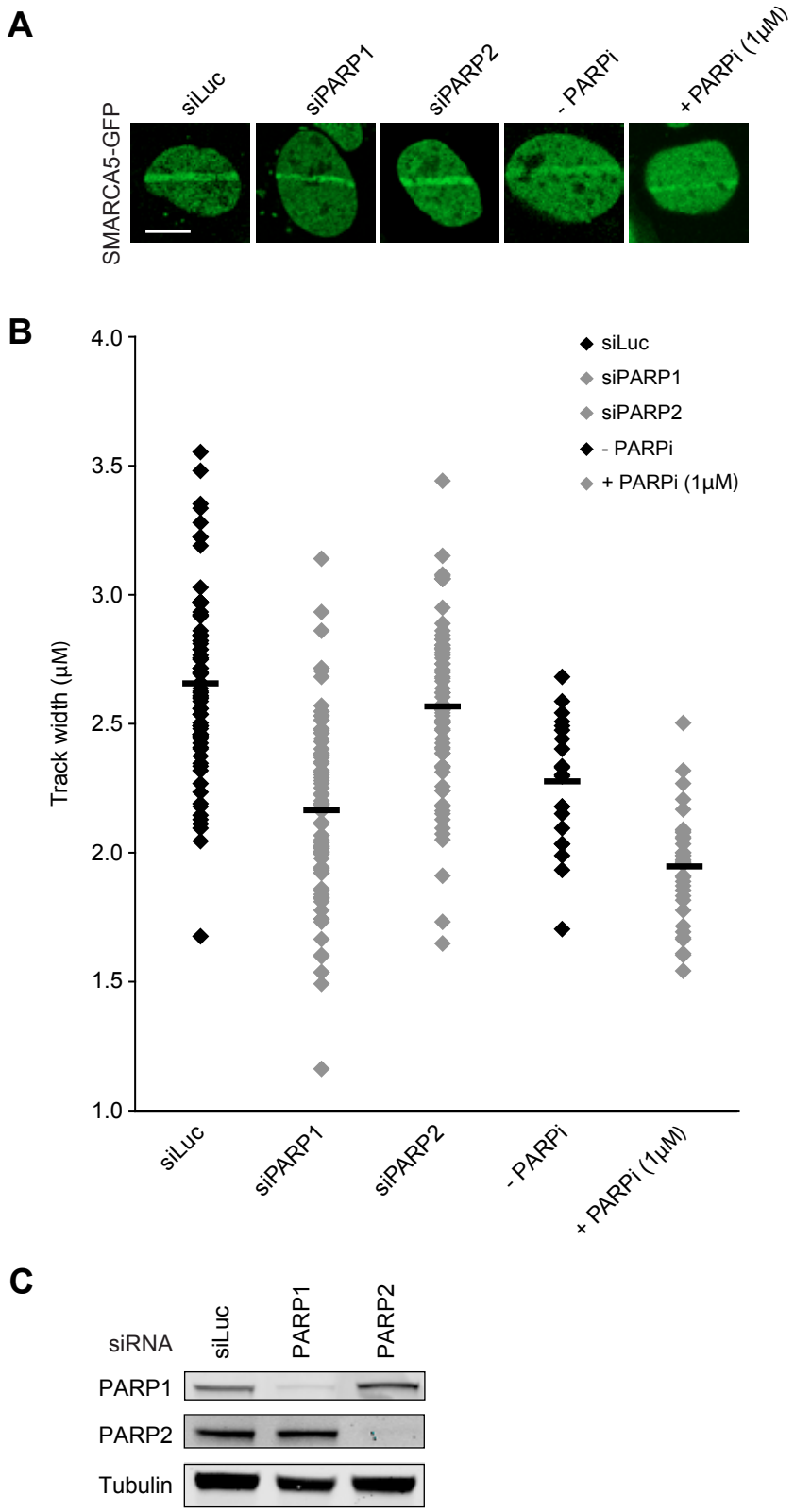

Fig. S6. PARP1, but not PARP2, distributes SMARCA5 throughout damaged chromatin. (**A**) Cells stably expressing SMARCA5-GFP were left untreated, transfected with siRNAs against PARP1 or PARP2, or treated with PARP inhibitor (1μM), then subjected to multi-photon laser-irradiation and analyzed for the expansion of SMARCA5-GFP throughout the damaged compartment. Representative images illustrating the effect of PARP1 knockdown, PARP2 knockdown and PARP1 inhibition (treatment of cells with 1 μM PARP inhibitor kills PARP1, but not PARP2 activity) on the expansion of SMARCA5 are shown. Scale bar, 10 μm. (**B**) Quantitative analysis of the width of DSB-containing laser tracks from cells in A. Laser tracks with a width of 1.5 μm were generated. After 180 s the width of the region showing accumulation of SMARCA5-GFP was measured to determine the increase in track width. Individual measurements ($n \geq 16$) and mean values are presented in a track-width distribution plot. (**C**) PARP1 and PARP2 levels were monitored by western blot analysis using whole cell extracts (WCE) of cells in A. Tubulin is a loading control.

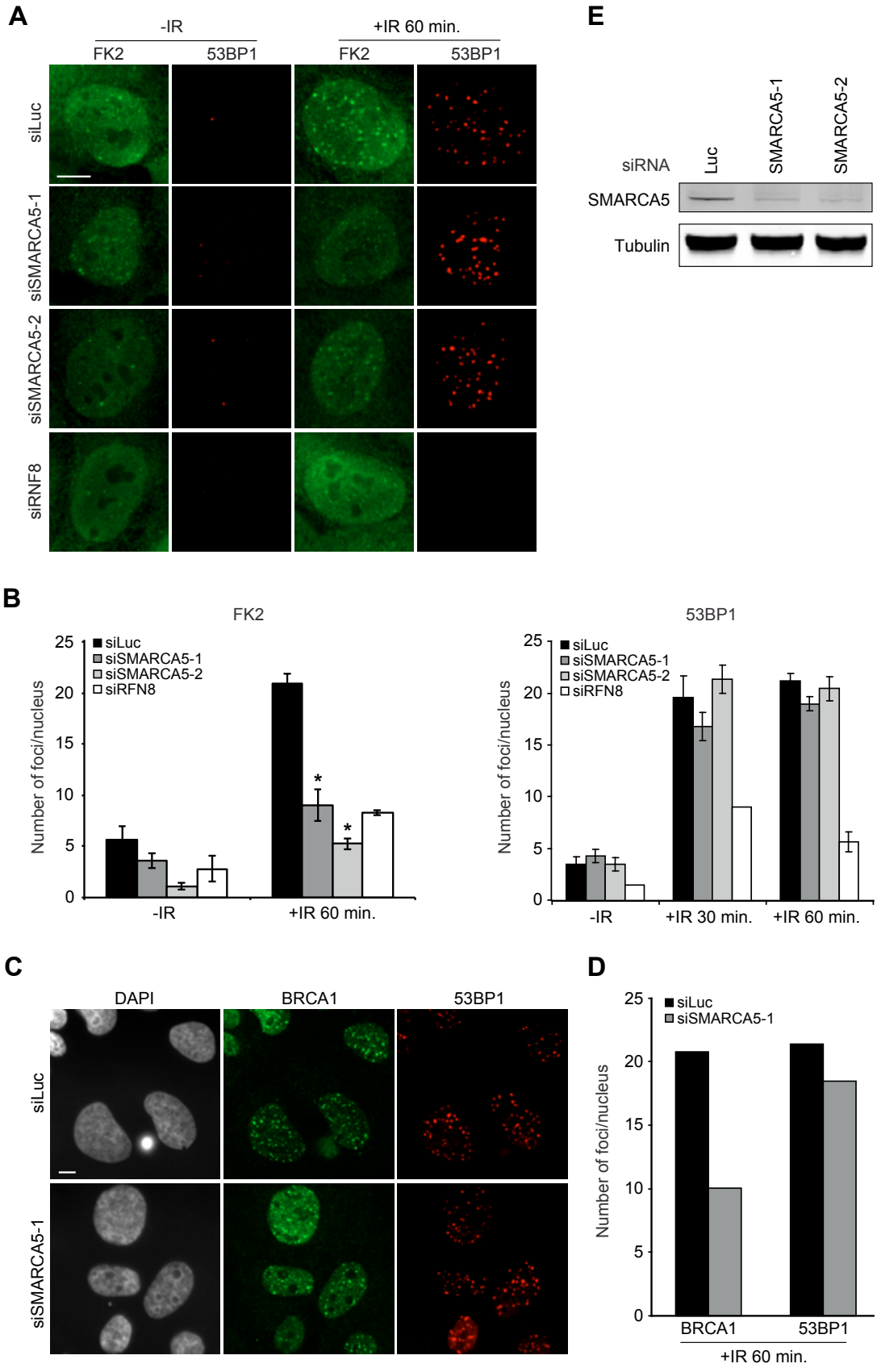

Fig. S7. SMARCA5 depletion does not affect53BP1 IRIF formation. (**A**) Cells were transfected with the indicated siRNAs, exposed to 1 Gy IR and 1 h later immunostained for conjugated ubiquitin (FK2) and 53BP1 to visualize IRIF. Scale bar, 10 μm. (**B**) Quantitative representation of FK2 and 53BP1 IRIF formation in A. The average number of foci/nucleus ± s.e.m. is presented. More than 150 nuclei were scored per time point in independent experiments. **P*<0.05, compared with siLuc (control). (**C**) As in A, except that cells were immunostained for BRCA1 and 53BP1. Scale bar, 10 μm. (**D**) As in B, except for cells from C. (**E**) SMARCA5 levels were monitored by western blot analysis using WCE of cells in A–D. Tubulin is a loading control.

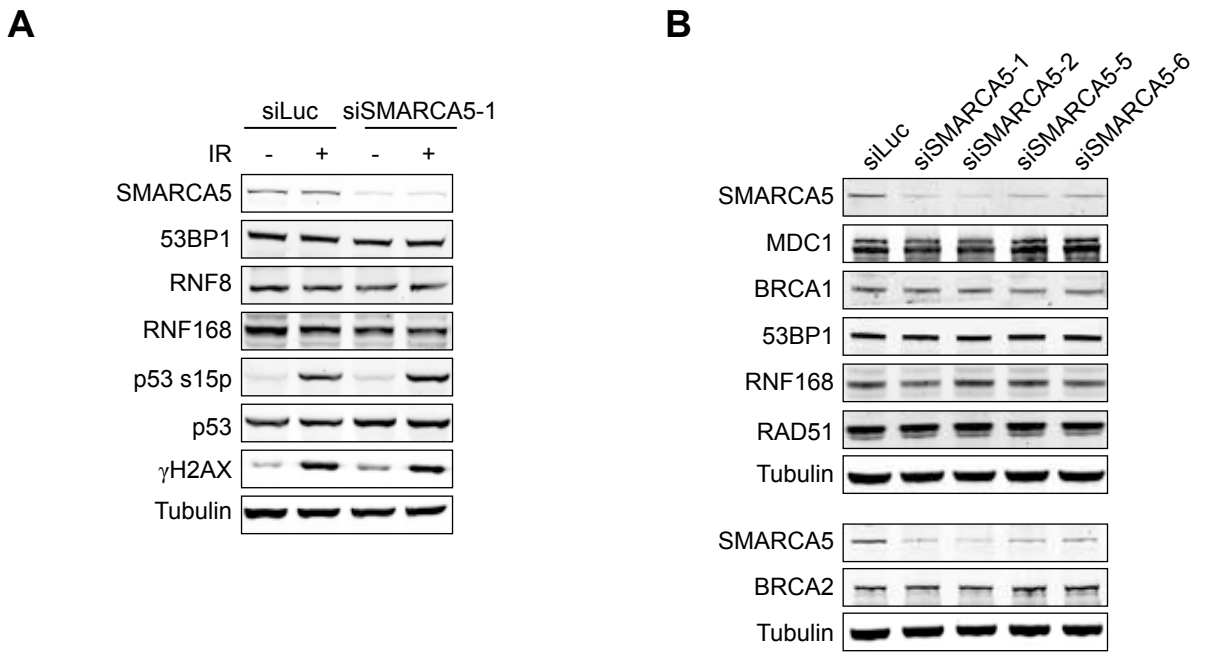

Fig. S8. SMARCA5 depletion does not affect the expression levels of DDR proteins. (**A**) SMARCA5 knockdown does not affect the expression levels of several DDR proteins. U2OS cells were transfected with the indicated siRNAs and left untreated or irradiated with 10 Gy IR. 1 h later WCE were prepared and protein levels were monitored by western blot analysis. Anti-53BP1 (Novus Biologicals), anti-p53 (Santa Cruz), anti-p53 S15p (Cell Signaling), anti-RNF8 (Abcam) and anti-BRCA2 (AB-1, Oncogene) antibodies were used. (**B**) As in A, except that cells were not irradiated.

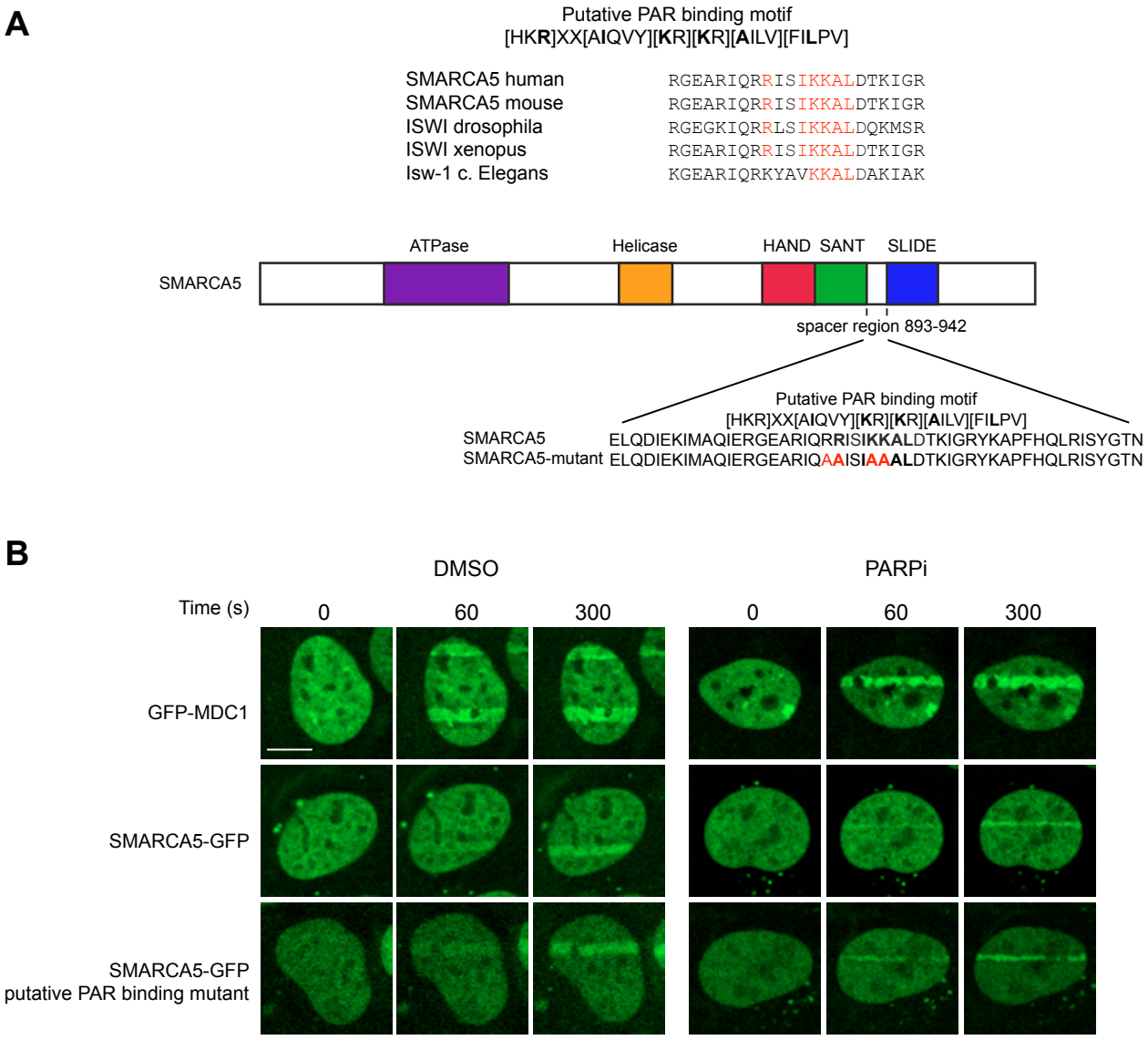

Fig. S9. The putative PAR binding domain of SMARCA5 is not required for its accumulation and spreading in damaged chromatin. (**A**) Schematic representation of the different functional domains in the SMARCA5 protein. A highly conserved putative PAR binding motif was found in the spacer region (893-943) located between the SANT and SLIDE domains. A SMARCA5 mutant was generated in which four conserved residues (two arginine residues and two lysine residues) in the putative PAR binding motif were substituted for alanine residues (indicated in red). (**B**) U2OS cells expressing GFP-MDC1, SMARCA5-GFP or the SMARCA5-GFP putative PAR binding mutant were treated with PARP inhibitor or left untreated and then subjected to multi-photon laser-irradiation. Scale bar, 10 μm.